Master thesis

A study on Stability of High-k Gate Thin Films in Moisture Ambience and Ultra-shallow Junction Technology by Plasma Doping Method

Supervisor
Professor Hiroshi Iwai
Associate Prof. Kazuo Tsutsui

Tokyo Institute of Technology
Department of Advanced Applied Electronics
01M36015
Sadahiro Akama

CONTENTS

Chapter 1

Introduction

1.1 Background

Today, IT (Information Technology), such as desktop application, mobile application and etc. has come into rapidly wide use recently, this is one of the most important technologies in our society. Development of IT owes to the improvement of semiconductor technology, mainly; Large Scaling Integrated circuits (LSIs) technology because there is no way about signal processing of GHz class at cheep, lightweight and low power without LSIs. Therefore Progress of IT must be greatly dependent on that of LSIs technology.

The progress of LSIs is caused by downsizing of devices, such as metal-oxide–semiconductor field effect transistors (MOSFETs) because high integration of the circuits become possible to carry many devices and to accomplish

multi-functionalization, then high performance such as high speed and high frequency wave is realized. The downsizing of MOSFETs has been accomplished by the scaling method as shown in Fig.1.1 and Table1.1 [1]. To increase the drive current and to control the short channel effects, these scaled transistors have to be designed very carefully. In this method, lateral and vertical dimensions and supply voltage are scaled down by the same factor S, while impurity-doping concentration is increased by the factor S.

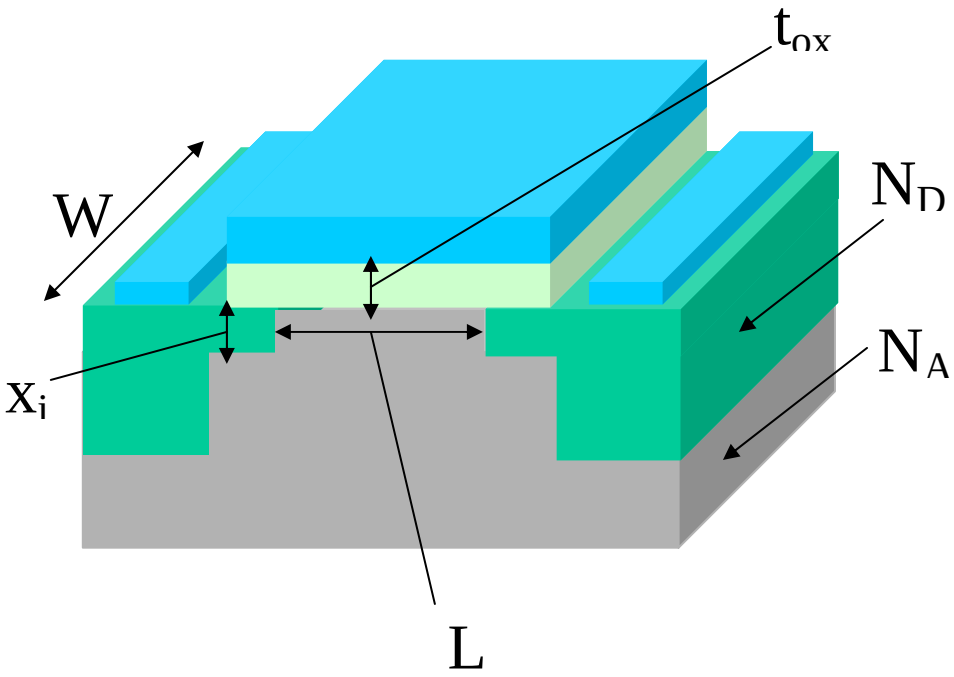

Fig.1.1 Over view of MOSFET

Table1.1 Scaling of MOSFET by scaling factor of S.

Quantity	*Before Scaling*	*After Scaling*
Channel Length	L	L/S
Channel Width	W	W/S
Device Area	A	A/S^2
Gate Oxide Thickness	t_{ox}	t_{ox}/S
Gate Capacitance (unit area)	C_{ox}	$S*C_{ox}$
Junction Depth	x_j	xj/S
Power supply voltage	V_{DD}	V_{DD}/S
Threshold Voltage	V_{T0}	V_{T0}/S
Doping Concentration	N_A	$S*N_A$
	N_D	$S*N_D$

1.2 Gate Insulator

1.2.1 Limits of SiO_2 gate insulator

Now, according to International Technology Roadmap for Semiconductors (ITRS) 2002 [2], as following scaling method, downsizing limits of MOSFET are rapidly approaching. As a result, the thickness of SiO_2 gate insulator decreases with decrease of gate length. In 2004, Equivalent of Oxide Thickness (EOT) reaches thinner than 1 nm as shown in Fig.1.2, and direct-tunneling leakage current is too increasing to be neglected as shown in Fig.1.3. Therefore SiO_2 gate insulator is to be replaced with an alternative material, which can be suppressed leakage current.

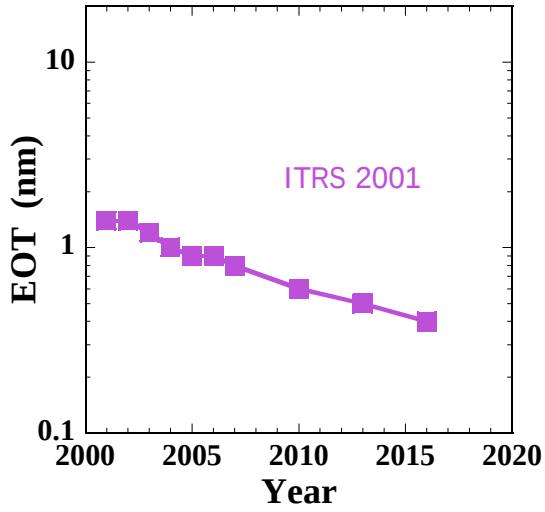

Fig.1.2 Trend of gate insulator thickness from ITRS roadmap 2001

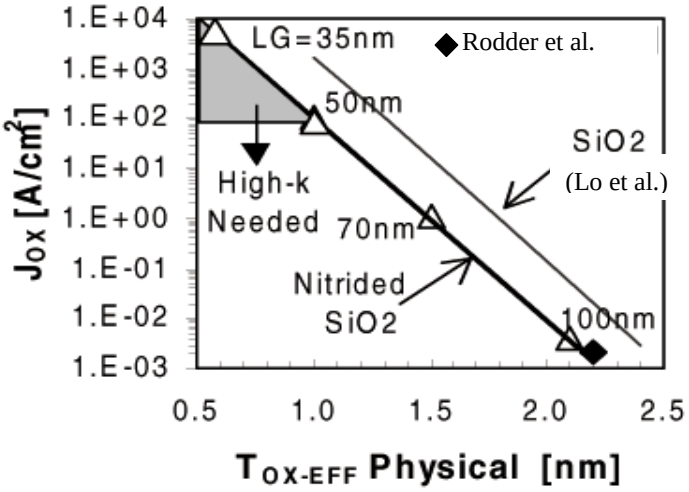

Fig.1.3 Relations between gate leakage current and physical thickness of SiO_2 film

1.2.2 Requirements for high-k gate insulator

Recently, especially 5 years later, the physical thickness of gate insulator is rapidly thinner, the present condition is having reached that of conventional SiO_2 gate insulator cannot be made more thin. Thus many researchers study new materials which have a dielectric constant higher than SiO_2 for gate insulator. A periodic table is shown in Table 1.2. White spaces are candidates for the oxide material, which is though to satisfy the above conditions in Table 1.4.

Table 1.2 Candidates for the metal, oxide of which has possibility to be used as high-k gate insulator on periodic table.

●=Not a solid at 1000 K
○= Radioactive
①=Failed reaction 1: $Si + MO_x \rightarrow M + SiO_2$
②=Failed reaction 2: $Si + MO_x \rightarrow MSi_x + SiO_2$
⑥=Failed reaction 6: $Si + MO_x \rightarrow M + MSi_xO_y$

● H																	● He
Li	Be											● B	● C	● N	● O	● F	● Ne
① Na	Mg											Al	Si	● P	● S	● Cl	● Ar
K	Ca	Sc	② Ti	① V	① Cr	① Mn	① Fc	① Co	① Ni	① Cu	① Zn	① Ga	① Ge	● As	● Se	● Br	● Kr
● Rh	Sr	Y	Zr	① Nb	① Mo	Tc	① Ru	① Rb	① Pd	● Ag	① Cd	① In	① Sn	① Sb	① Te	● I	● Xe
● Cs	⑥ Ba	R	Hf	① Ta	① W	① Re	① Os	① Ir	● Pt	● Au	● Hg	● Tl	① Pb	① Bi	○ Po	○ At	○ Rn
○ Fr	○ Ra	A	○ Rf	○ Ha	○ Sg	○ Ns	○ Hs	○ Mt									

R	La	Ce	Pr	Nd	○ Pm	Sm	Eu	Gd	Tb	Dy	Ho	Er	Tm	Yb	Lu
A	○ Ac	○ Th	○ Pa	○ U	○ Np	○ Pu	○ Am	○ Cm	○ Bk	○ Cf	○ Es	○ Fm	○ Md	○ No	○ Lr

The capacitance equation of gate insulator is as follows;

$$C = \frac{\varepsilon_0 \varepsilon S}{d} \tag{1.1}$$

Where ε_0, ε, S and d are vacuum dielectric constant, the relative dielectric constant, area size of the top electrode and thickness of gate oxide films. The capacitance of gate insulator remains if the relative dielectric constant is 10 times even if oxide thickness is 10 times. Thus the application of high-k gate insulator should enable usage of thicker films of equivalent SiO_2 electrical thickness with expected reduction in leakage current and improved gate reliability as shown in Fig.1.4.

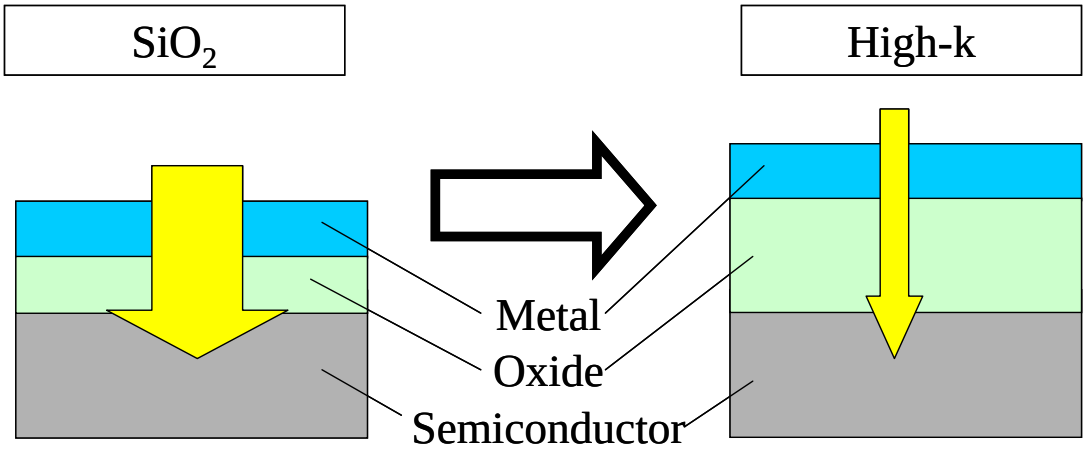

Fig1.4 leakage current for alternative high-k gate insulator

Table 1.3 shows major high-k materials. There are many reports about silicate, SiO_xN_y, Al_2O_3, HfO_2, ZrO_2 and rare earth oxide like La_2O_3, Pr_2O_3, Gd_2O_3 and Yb_2O_3 (Fig.1.5). Al2O3 has good thermal stability. So it is not easy to react with Si substrate and has no problem in high temperature process in integration of the MOSFETs. But it has a lot of fixed oxide charges and smaller than permittivity than any other high-k material. HfO2 and ZrO_2 are easily reacted with Si to form SiO_2, silicates and/or silicides. Moreover, these materials are easy to be crystallized. (HfO_2 and ZrO_2 are crystallized over 700^{o}C and 400^{o}C, receptivity.) Thus, it is too serious for these materials to increase the leakage current because of crystallization. The rare earth oxides have one of the highest permittivity in high-k materials. Recently, excellent results of these materials, such as La_2O_3 and Pr_2O_3, have been reported, while these materials have been some problems [3-9]. These are easy to form silicate for heat process, and the most fatal problems of these are stability in air.

Table 1.3 Major high-k material properties

Materials	SiO_2	Al_2O_3	La_2O_3	HfO_2	ZrO_2
Contact stability with Si (kJ/mol) $Si + M_{ox} \rightarrow M + SiO_2$	Stable	+63.4	+98.5	+47.6	+42.3
Lattice Energy (kJ/mol)	13125	15916	12687		11188
Band Gap (eV)	9	6 – 8	5.4	5.7	5.2 – 7.8
Permittivity	3.9	8.5 – 10	27	24	11 – 18.5
Structure	Amorphous	Amorphous	Amorphous	Crystal T > 700°C	Crystal T > 700°C

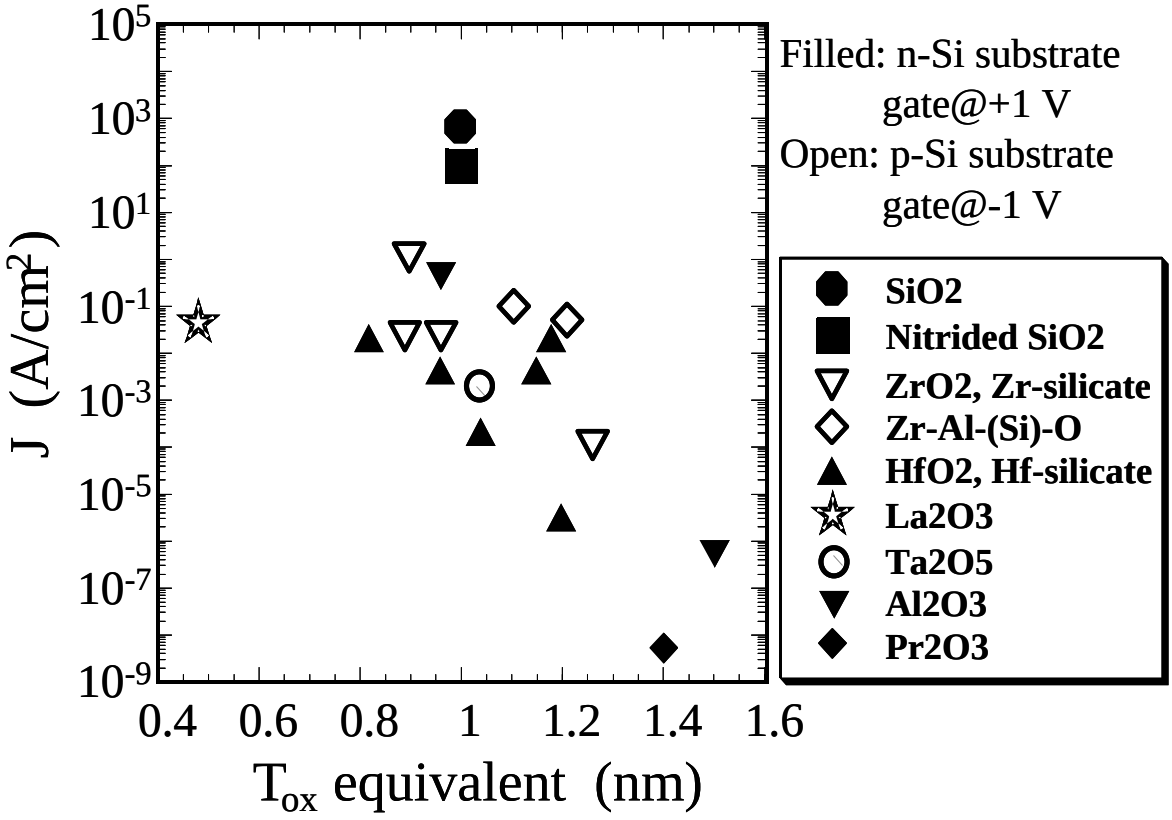

Fig.1.5 J vs. Leakage Current Density plot of Varies high-k materials

1.2.3 Physical properties of rare earth oxides

In general, the rare earth oxides become hydroxide and carbonate in H_2O and CO_2 ambient [10]. Figure 1.6 and 1.7 show reaction about the generation of hydroxide and carbonate, respectively. It is said that entire rare earth oxides become gradually hydroxide in H_2O, while only the surface become carbonate in CO_2 at room temperature and the pressure of the atmosphere. However heavy rare earth oxide is a little change. Figure 1.8 shows stability of La_2O_3 ceramics in clean room air for 30 hours. It became in pieces and expand.

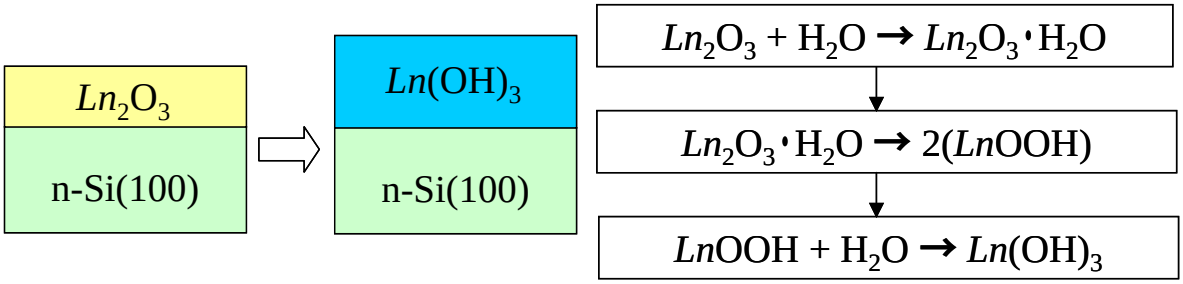

Fig.1.6 Schematic of the hydroxide's generation

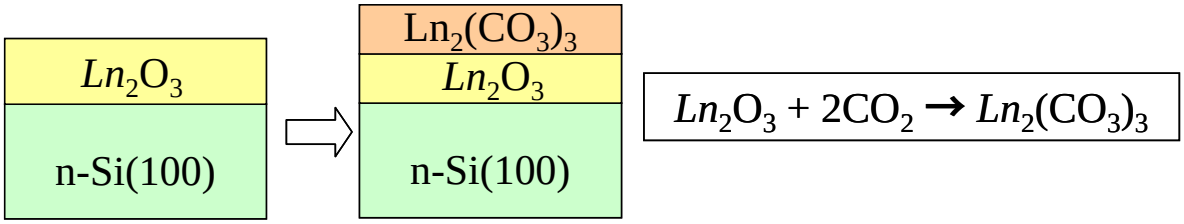

Fig.1.7 Schematic of the carbonate's generation

Fig.1.8. La2O3 ceramics (The picture of the left hand is initial, and that of the right hand is after 30 hours in clean room.)

Figure 1.9 shows lattice energy and band gap of rare earth oxides. And Table 1.4 shows the boiling and melting point of rare earth oxides. Lattice energy is increase with the decrease of the rare earth oxides ion's radius. Therefore heavy rare earth oxides react smaller because of film crystallization.

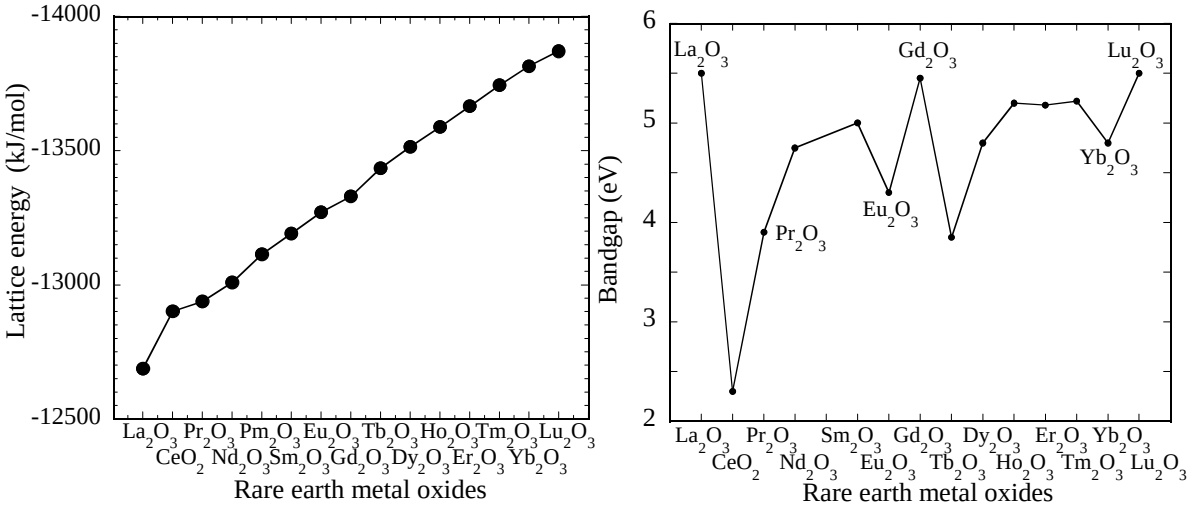

Fig.1.9 lattice energy and band gap of rare earth oxides

Table 1.4. The melting and boiling point of the rare earth oxides, respectively

Materials	The melting point (°C)	The boiling point (°C)	Materials	The melting point (°C)	The boiling point (°C)
La_2O_3	2256	3620	Gd_2O_3	2339	3900
	2304±5		Tb_2O_3	2303	
Ce_2O_3	2210±10	3730	Dy_2O_3	2228	3900
Pr_2O_3	2183	3760	Ho_2O_3	2330	3900
Nd_2O_3	2233	3760	Er_2O_3	2344	3920
Pm_2O_3	2320		Tm_2O_3	2341	3945
Sm_2O_3	2269	3780	Yb_2O_3	2355	4070
Eu_2O_3	2291	3790	Lu_2O_3	2427	3980

1.3. Junction

1.3.1 Requirements and problems for shallow junction

The downsizing of MOSFET progresses rapidly by the scaling method. Consequently, length between source and drain is nearly in other words, channel length becomes shorter, and various inconvenient influences called short channel effect is appeared. In order to suppress problem to of short channel effect to the minimum, it is necessary to make shallower junction and to hold behavior of a long channel. While, it is necessary to suppress raising maximum drain extension sheet resistance. According to ITRS roadmap 2002 as shown in Table 1.5 and Fig.1.10, junction depth is 13-22 in 2005 year and 7-12 in 2010 year [2]. However, as concerns conventional ion implantation technology, cost is high and control of low energy is difficult. Therefore, new ultra-shallow junction formation technology is demanded.

Table 1.5 ITRS roadmap 2002

Year of production	2002	2005	2007	2010	2016
Physical Gate Length (nm)	53	32	25	18	9
Drain extension Xj (nm)	22-36	13-22	10-17	7-12	4-6
Max. drain extension sheet resistance (Ω/sq.)	460	770	760	830	1210

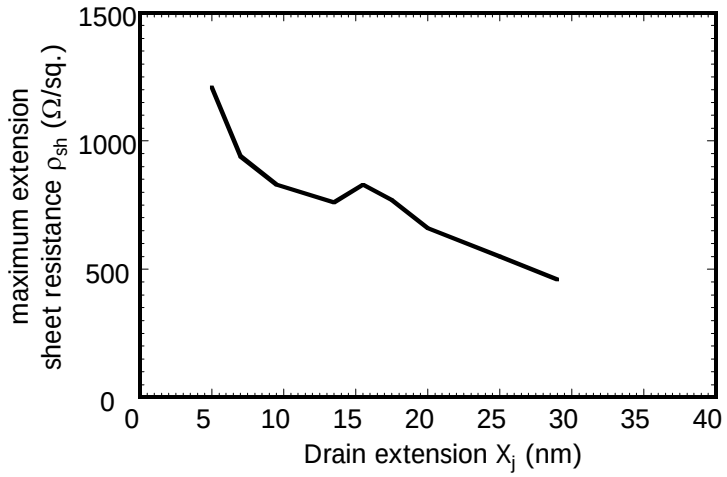

Fig.1.10 Roadmap for X_j vs. ρ_{sh} ITRS'2002

1.3.2 Requirement for plasma doping (PD) method

In these years, as rapidly downsizing, conventional ion implantation technology is too difficult to control low energy implantation for ultra-shallow junction formation. And so, establishment of new ultra-shallow junction technology is required [11-13]. Plasma doping (PD) method is expected as the low cost and high performance technology as follows,

Possibility to control of implantation by low energy

High throughput

Compact system

Excellent characteristics of transistor.

Another advantage of PD method can be given isotropy and anisotropy. Herewith, 3-dimention formations such as trench sidewall can be doped.

While demerit of PD method compared with ion implantation method have as follows;

Substance without mass separation reaches Si wafer

The exact amount of ion using Faraday cup cannot be measured because only positive ion doesn't always reach Si wafer. However, neither problem is fatal. Although the former problem may have a bad influence on transistor operation, it already has report of operating one. On the other hand, although the latter problem has the point that dosage isn't known simply, simple measurement for dosage is becoming impossible in case of low energy by ion implantation method because the problem such as sputtering and back sputtering is not neglected within ultra-shallow junction. Therefore, According to ITRS roadmap 2002, PD method is expected as low energy technology as shown in Fig.1.11 in future [2].

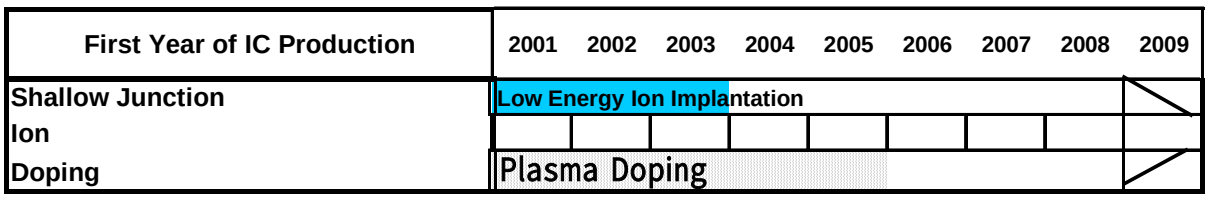

Fig. 1.11 IRTS roadmap 2001

Figure 1.12 shows Boron depth profile by SIMS in case of using conventional ion implantation method and plasma doping method [14]. In the vicinity of surface, Boron concentration in case of using plasma doping method was strong that of in case of using conventional ion implantation. It is guessed that this phenomenon is absorption of Boron in neighbor of Si surface due to reacting absorption of gas phase.

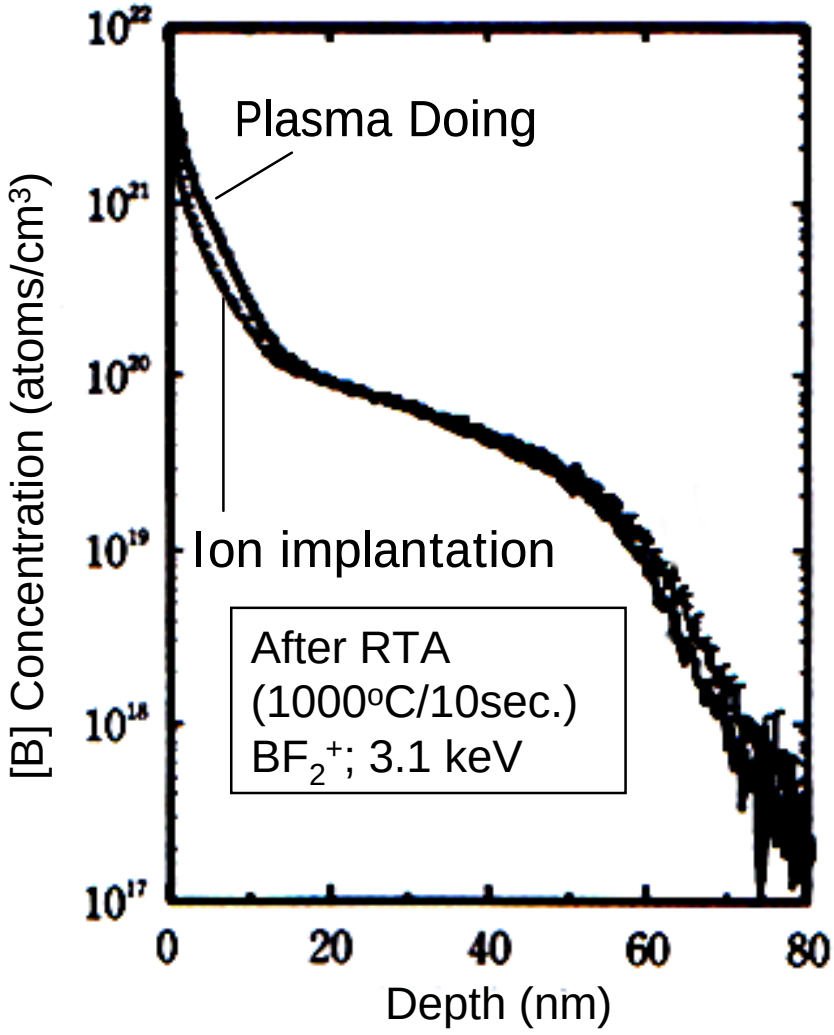

Fig.1.12 Boron depth profile by SIMS in case of using conventional ion implantation method and plasma doping method

1.4 Purpose of This Study

1.4.1 Stability of high-k gate thin films in moisture ambience

Among the high dielectric constant materials, excellent results of those materials have been reported, nevertheless, for the rare earth oxides, moisture absorption is the biggest concern. However, there has been no other report about this problem so far. The purpose of this study is to confirm whether it has a possibility to be use gate insulator for the next generation MOSFETs from the examination of the stability of high-k gate thin films by moisture absorption test.

1.4.2 Ultra-shallow junction Technology by plasma doping method

PD method which can be given low ion energy due to controlling bias energy is attracted because conventional beam line ion implantation method is too difficult to control low acceleration voltage. However, the investigation about ion implantation technology which can be given low energy is carried out vigorous, research using the plasma doping method is seldom done. And so, investigation of reacting absorption of gas phase was hardly carried out. Therefore, the purpose of this study is to strive to establish mechanism about ultra-shallow junction formation technology in next generation by using PD method.

Chapter2

Fabrication and Characterization Methods

2.1 Fabrication methods

In this sub section, the fabrication methods for MIS (Metal-Insulator-Semiconductor) are discussed.

2.1.1 Cleaning of Si substrate

Prior to deposit of high-k gate thin films for LSI fabrication process; (for example, MIS capacitors at this study), the ultra-pure surface of a bare Si substrate should be chemically cleaned to remove particles contamination, such as metal contamination, organic contamination, ionic contamination, water absorption, native oxide and atomic scale roughness. It is considered that this substrate cleaning process is too important to realize desirable device operation and its reproducibility.

In full fabrication processes as well as substrate cleaning, DI (de-ionized) water is one of the most important because DI water is highly purified and filtered to remove all traces of ionic, particulate, and bacterial contamination. Theoretical resistively of pure water at 25^{o}C is 18.3 MΩ·cm. The resistively value of ultra-pure water (UPW) used in this study achieve more than 18. 2 MΩ·cm and have fewer than 1.2 colony of bacteria per milliliter and no particle larger than 0.25um.

In this study, the method of substrate cleaning process was used a typical processing using hydrofluoric acid, which is usually called RCA cleaning method, was proposed by W. Kern et al. But some steps were reduced. The steps were shown in Fig.2.1. Firstly, a cleaning steps in solution of sulfuric acid (H_2SO_4) / hydrogen peroxide (H_2O_2) (H_2SO_4:H_2O_2 = 1:4, called by SPM) performed to remove any organic material and metallic impurities after UPW cleaning. Secondly, the step in a solution of dilated hydrofluoric acid (HF:H_2O = 1:100) was performed to remove chemically and native oxides which might have been formed on Si surface. Final step was dipped in UPW because hydrogen-terminated surface.

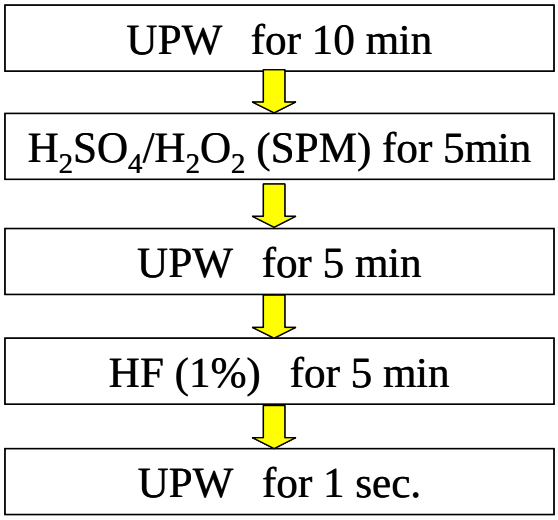

Fig.2.1 Si surface cleaning process

2.1.2 Molecular beam deposition (MBD)

MBD (Molecular Beam Deposition) method is the thin film formation method which is made a target of the materials the shape of the beam, evaporated and deposited that of materials on Si substrate in 10^{-10} Torr or less ultra-high vacuum. The characteristic of that method can make a good film formation without contamination because of preventing the discharge from circumference due to covering with panel which is cooled by liquid N_2 in vacuum chamber.

Fig.2.2 and Fig.2.3 show the schematic drawing of the equipment, which was used in this study. There are two chambers, such as loading and growth chamber, four E-guns in deposition chamber, RHEED (Reflection High-Energy Electron Diffraction), and two power supplies that are capable to evaporate two materials in the same time. (But one E-gun was used in this study.) The pressure in loading chamber is about 10^{-8} Torr by a rotary pump connected to a turbo molecular pump. The background pressure in growth chamber is about 10^{-10} Torr by a ion pump. During deposition, the pressure is 10^{-9} to 10^{-7} Torr.

In the growth chamber, a target of high-k material is evaporated by e-beam accelerated voltage of by –5kV. And then high-k thin film is deposited on the Si substrate. The substrate rotates 10rpm (revolutions per 1 minute) to uniform the film thickness.

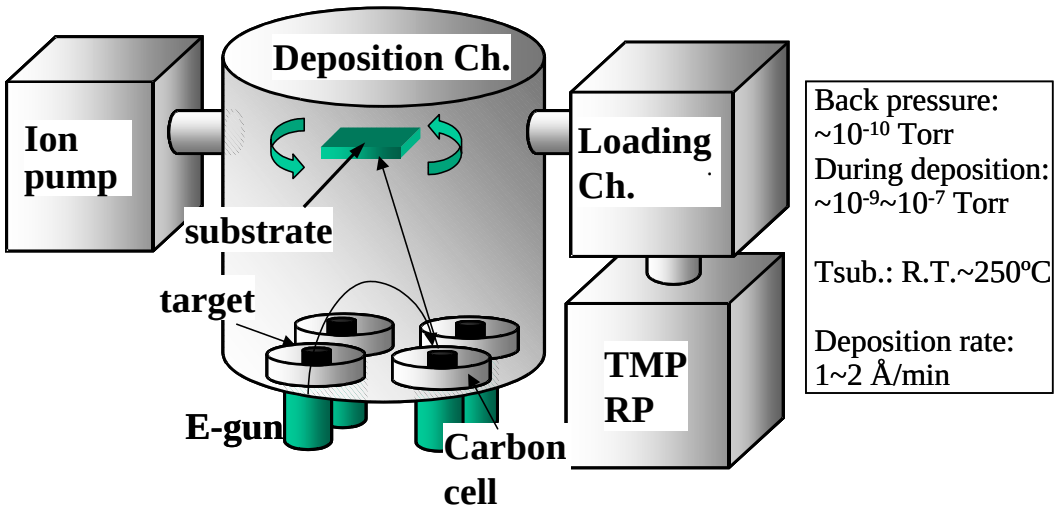

Fig.2.2 Schematic drawing of the MBD chamber

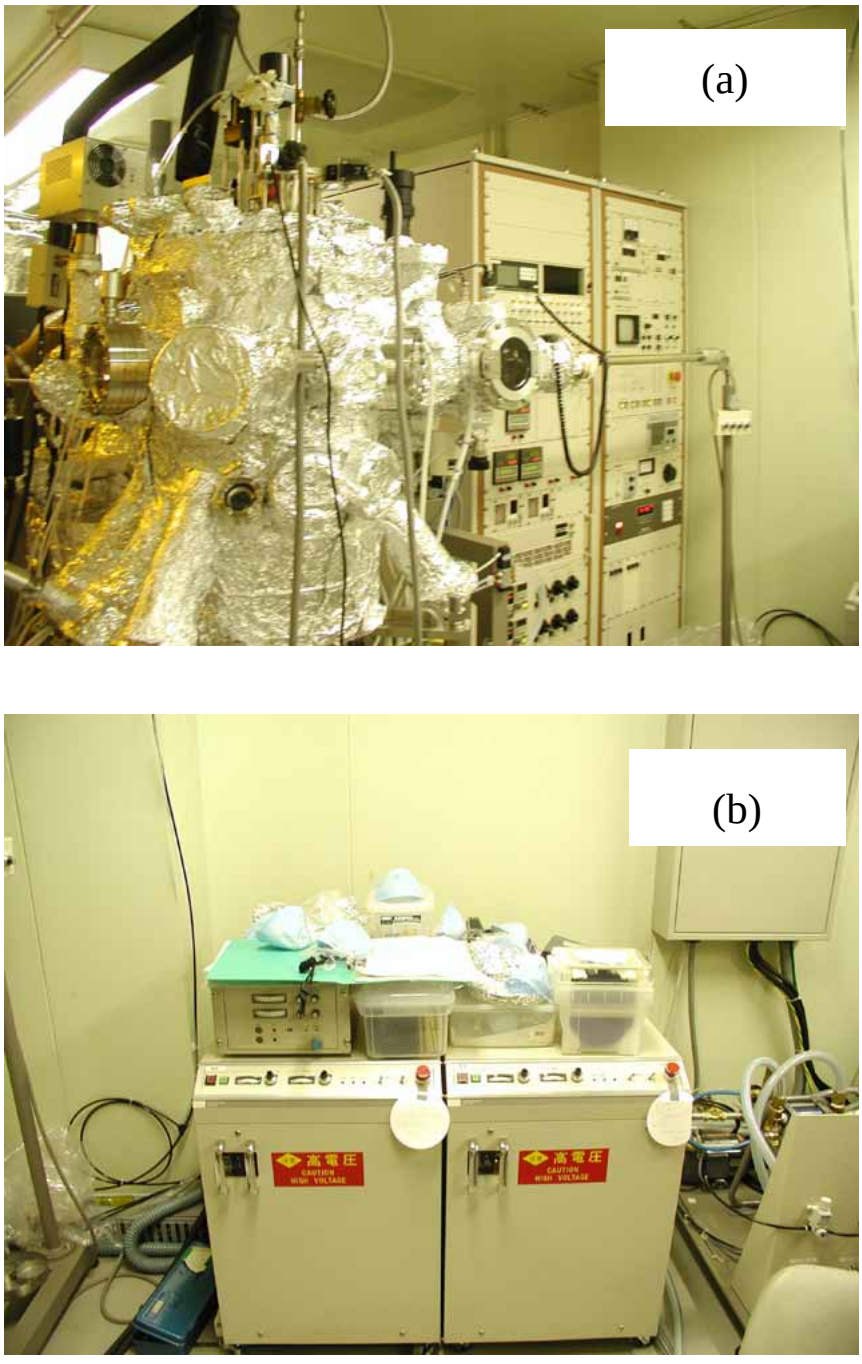

Fig.2.3 (a) MBD chamber and (b) power supplies

2.1.3 Rapid thermal annealing (RTA)

Annealing process is needed one of the most important processes because of removing trap electrical charge into oxide films and recovering mobility and parameters of the other material due to activating ion after doping. In this study, RTA (Rapid Thermal Annealing; MILA-3000) as shown in Fig.2.3 is used to anneal samples that is deposited oxide film or doped impurities.

This RTA system has a heating method which fixes a lamp of infrared light to spot of a parabolic refractor of and then is reflected an infrared light in parallel. The furnace temperature can be raised from Room Temperature (R.T.) to 1200 ^{o}C. Rate of temperature increase is same value or less than 50 ^{o}C/sec. Annealing is carried out in N_2 or O_2 ambient by running gas into furnace at atmospheric pressure. This system cannot be vacuumed and so completely be replaced by the gas.

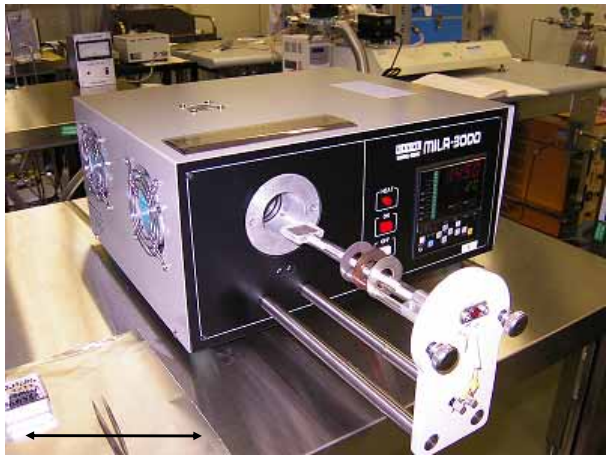

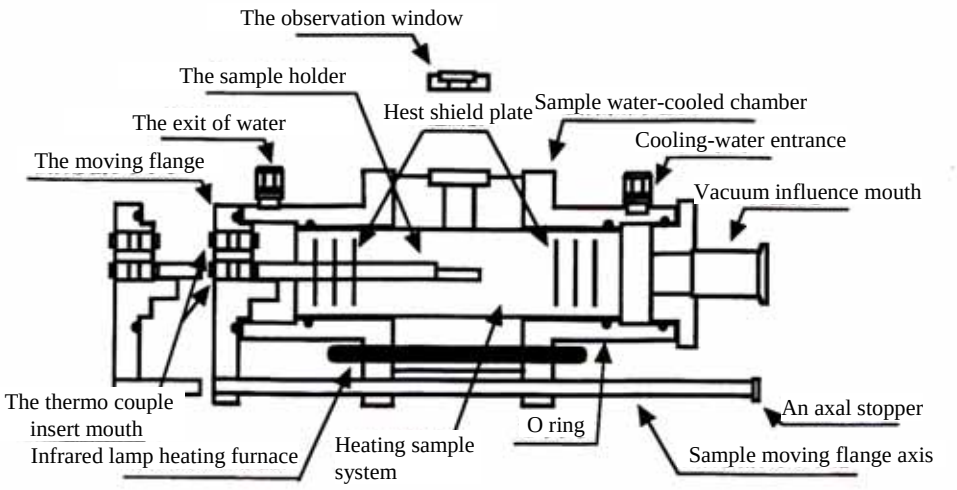

Fig. 2.3 (a) Photo and (b) The schematic overview of RTA (MILA-3000) system

2.1.4 Vacuum evaporation method

The Al electrode is deposited on the top and bottom on n type Si substrate by a vacuum evaporation system with a bell jar as shown in Fig.2.4. We use an Al source which has a purity of 99.999 % value. A filament made of tungsten is used for thermal heating Al source and Al electrode is deposited on Si substrate. During deposition, the pressure is around 10^{-5} Torr by vacuuming turbo pump.

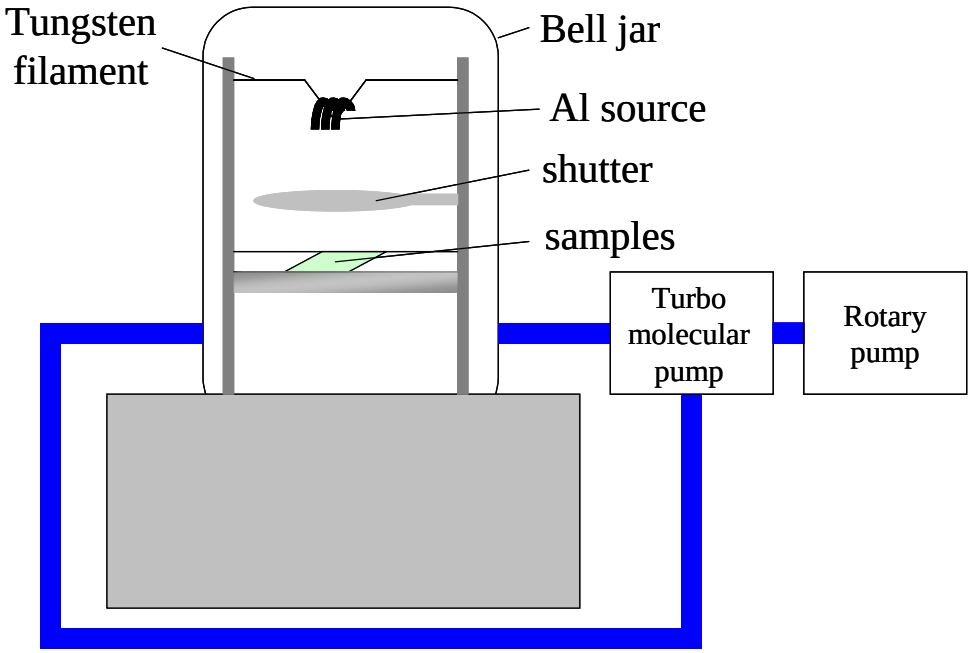

Fig, 2.4 (a) Photo and (b) schematic overview of vacuum evaporation system

2.1.5 Experimental apparatus for moisture absorption test

Figure 2.5 shows experimental apparatus for moisture absorption test. Ultra-pure water was used as the moisture supply. The effect of desorption gas from the moisture absorption test apparatus was investigated by the apparatus made of acryl (PMMA : $CH_2C(CH)_3COOCH_3$) and glass (PYREX). The temperature and humidity were maintained at 25°C and 80%, respectively.

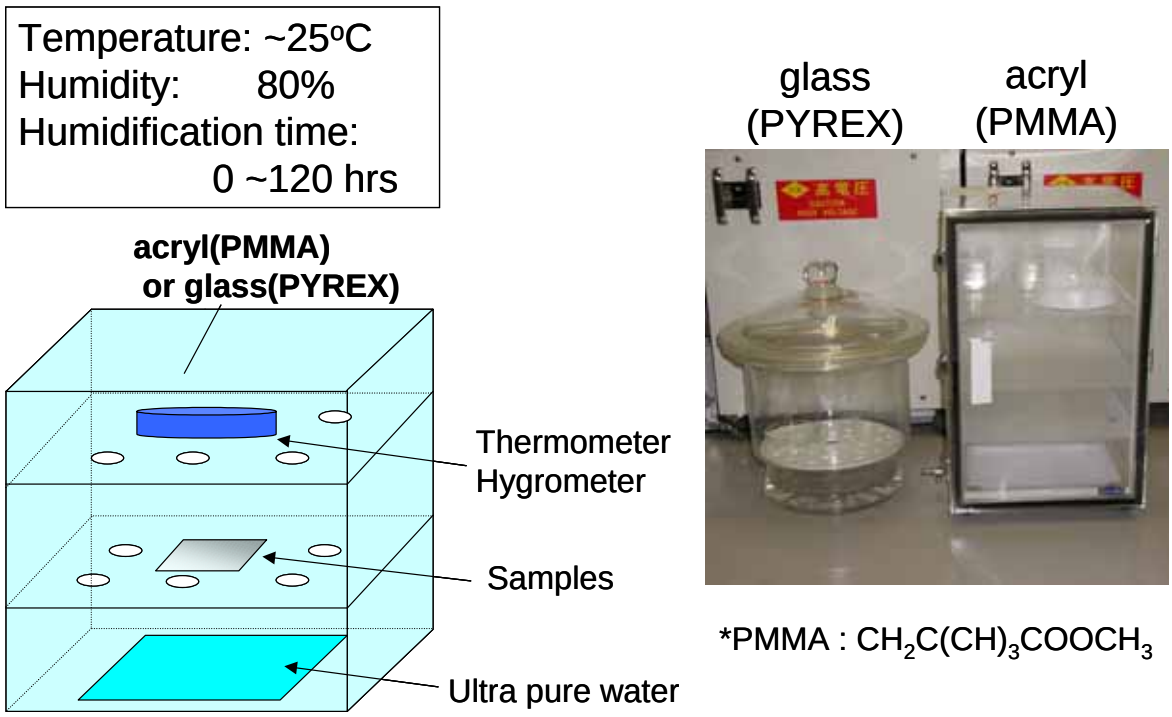

Fig.2.5 Experimental apparatus

2.1.6 Plasma doping system

In Plasma doping, the intermediate stages of ion source, beam extraction, focusing, and scanning are omitted. The target is immersed in a plasma environment, and ions are extracted directly from the plasma and accelerated into the target by means of a series of negative high-voltage pulses applied to the target.

Figure 2.6 and Fig.2.7 shows schematic and Photo of Plasma Doping System, respectively. There are two chambers, such as loading and process chamber, two rf-power supplies (13.56MHz), such as source and bias power supply, and Langmuir probe in order to measure plasma characteristics. This system has characteristic of low-pressure and high-density plasma source by helicon source. Helicon source has characteristics that a weak (50-200G) dc axial magnetic field together with an rf-driven antenna placed around of a helicon wave within the source plasma, and then resonant wave-particle interaction is believed to transfer the wave energy to the plasma. In addition to high-density and low-pressure, a feature is that the rf-power is coupled to the plasma across a dielectric window, rather than by direct connection to an electrode in the plasma, as for an rf-diode. When a sudden negative voltage $-V_0$ is applied to the target, then, leaving behind a uniform-density ion matrix. In pressure in loading chamber is about 10^{-2} Pa by a rotary pump connected to a turbo molecular pump. The background pressure in process chamber is about 10^{-5} Pa or less by a turbo molecular pump. During doping, the pressure is 0.1 to 2.5 Pa.

In the process chamber, Argon (Ar), Helium (He), and di-borane (B_2H_6) is introduced and is discharged by source power supply. And then target ion is doped by accelerated ion by bias power supply connected electrode under wafer holder.

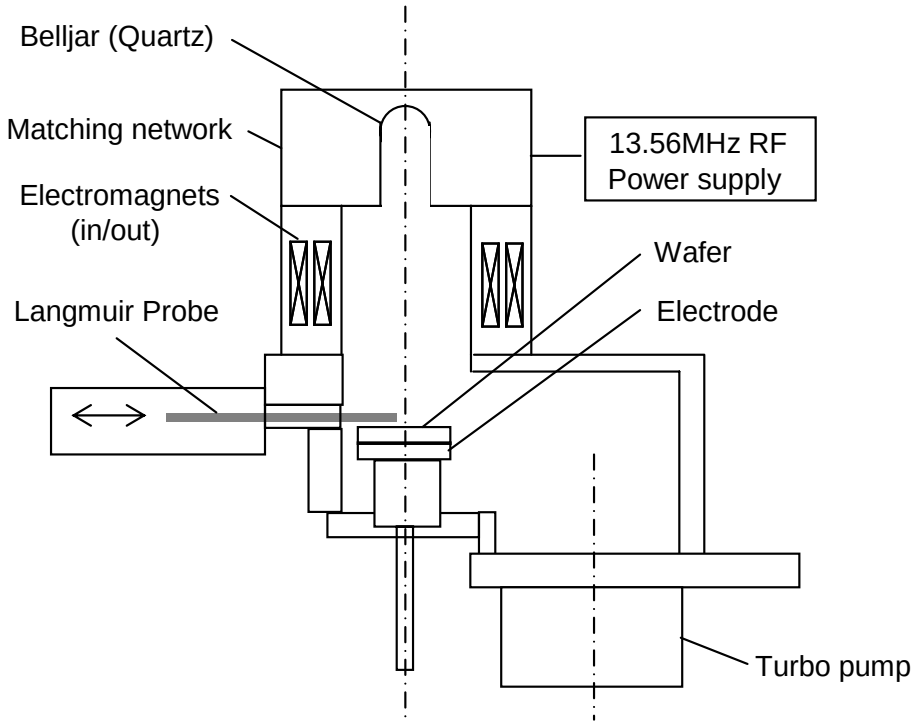

Fig.2.6 Cross section of Plasma Doping equipment. Plasma source, reactive chamber and wafer handling system are installed.

Fig.2.7 Photo of Plasma Doping system

2.2 Analysis methods

In this sub section, varies analysis methods for MIS are discussed.

2.2.1 Principles and measurements of electrical characteristics

2.2.1.1 C-V (Capacitance-Voltage) characteristics

Figure 2.8 shows the ideal of C-V characteristic of p-type MOS diode. Here, "ideal" MOS diode means that there is no interface-trapped charge (Q_{it}), fixed charge (Q_f), oxide trap charge (Q_{ot}) and mobile ion charge (Q_m). The total capacitance (C) of MOS diode equals the oxide capacitance (C_0) which is accumulated and the silicon capacitance (C_{Si}) connected in series as follows,

$$C = \frac{C_0 C_{Si}}{C_0 + C_{Si}} \quad (\mathrm{F/cm^2}). \tag{2.1}$$

And we obtain

$$\frac{C}{C_0} = \frac{1}{\sqrt{1 + \frac{2\varepsilon_{ox}{}^2 V}{qNA\varepsilon_{si}d^2}}}, \tag{2.2}$$

where we have written out C_{Si} explicitly. This equation indicates that the capacitance decreases with increase of the gate voltage.

If applied voltage is negative, depletion layer is not generated but hole is accumulated in surface of silicon. As a result, the total capacitance equals approximately the oxide capacitance (ε_{ox}/d). Beyond strong inversion, even if the voltage increases more than that, the thickness of depletion layer doesn't increase any longer. The gate voltage is called *threshold voltage (V_T)* in this condition as follows.

$$V_T = \frac{\sqrt{2\varepsilon_{Si} q N_A (2\psi_B)}}{C_0} + 2\psi_B, \tag{2.3}$$

moreover, capacitance is as follows

$$C_{\min} = \frac{\varepsilon_{ox}}{d + (\varepsilon_{ox} / \varepsilon_{Si}) W_m}. \tag{2.4}$$

In conventional MOS diode, however, the difference of work function between metal and oxide (ϕ_{ms}) is not zero and there are varies space charges, such as Q_{it}, Q_f, Q_{ot} and

Q_m, in oxide and interface of oxide-semiconductor, therefore those affect characteristics of ideal MOS diode. As a result, flat band voltage (V_{FB}) is shifted from ideal that as follows,

$$V_{FB} = \phi_{ms} - \frac{Q_f + Q_m + Q_{ot}}{C_0}. \tag{2.5}$$

And C-V carve is parallel shifted as shown in Fig.2.5 (b) because ϕ_s, Q_m, Qot is not zero. And addition to that, when there are much Q_{it}, that is changed by surface potential. Therefore, curve (c) as shown in Fig.2.5 is shifted and bended by Q_{it} value.

CET (Capacitance equivalent thickness) in other words, T_{ox} electrical equivalent means the thickness of equivalent SiO_2, can be calculated from accumulated capacitance of C-V characteristic as follows,

$$CET = \varepsilon_0 \varepsilon_{Si} \frac{S}{C_0}, \tag{2.6}$$

where ε_0, ε_{Si} and S are permittivity of vacuum, dielectric constant of SiO_2 and area of a capacitor.

In this study, HP4284A (Hewlett-Packard Co. Ltd.) is used for measurement C-V characteristic. The range of measurement frequency is 1 to 10MHz.

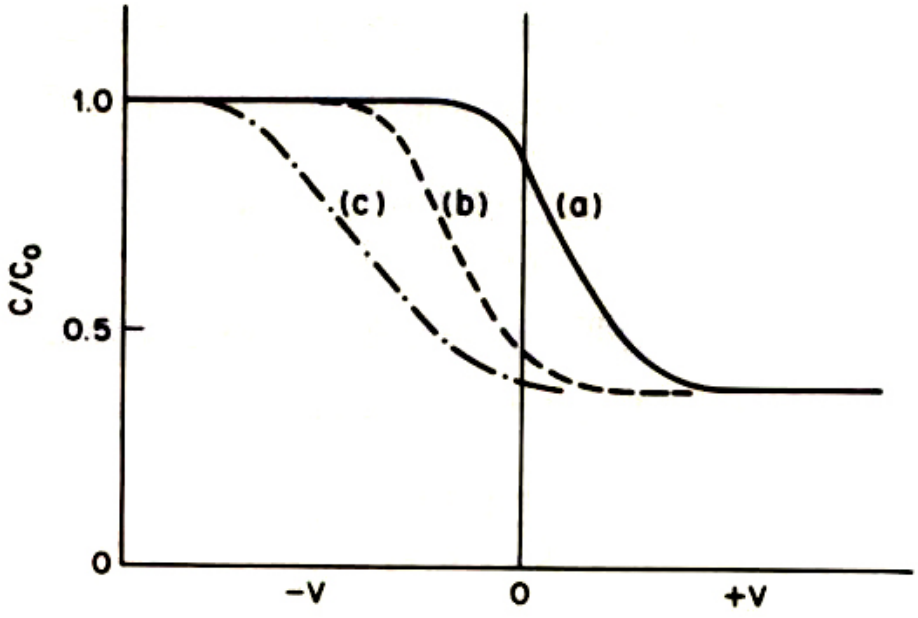

Fig.2.8 the ideal of C-V characteristic of p-type MOS diode

2.2.1.2 J-V (Current Density-Voltage) characteristics

It is important to suppressed the leakage current of the gate dielectric film as small as possible in order to lower the power consumption of LSI. To estimate the leakage, J-V characteristics are measured using semiconductor-parameter analyzer (HP4156A, Hewlett-Packard Co. Ltd.)

2.2.2 Atomic Force Microscopy (AFM)

The surface roughness of the film is evaluated by Atomic force microscopy (AFM, Nano Scope 3, Digital Instrument Co. Ltd.) in tapping mode.

Figure2.9 shows principle of tapping mode AFM. Tapping mode AFM accelerates cantilever with probe at the tip near resonant frequency, and so scan surface of the film tapping lightly intermittently. The distortion is detected by a variation of reflection angle of laser beam which is irradiated to the cantilever. The distance is controlled to keep the distortion constant while scanning in x and y directions and the control of the distance in z direction. Spatial resolution of AFM used in this study is around 1.0 nm.

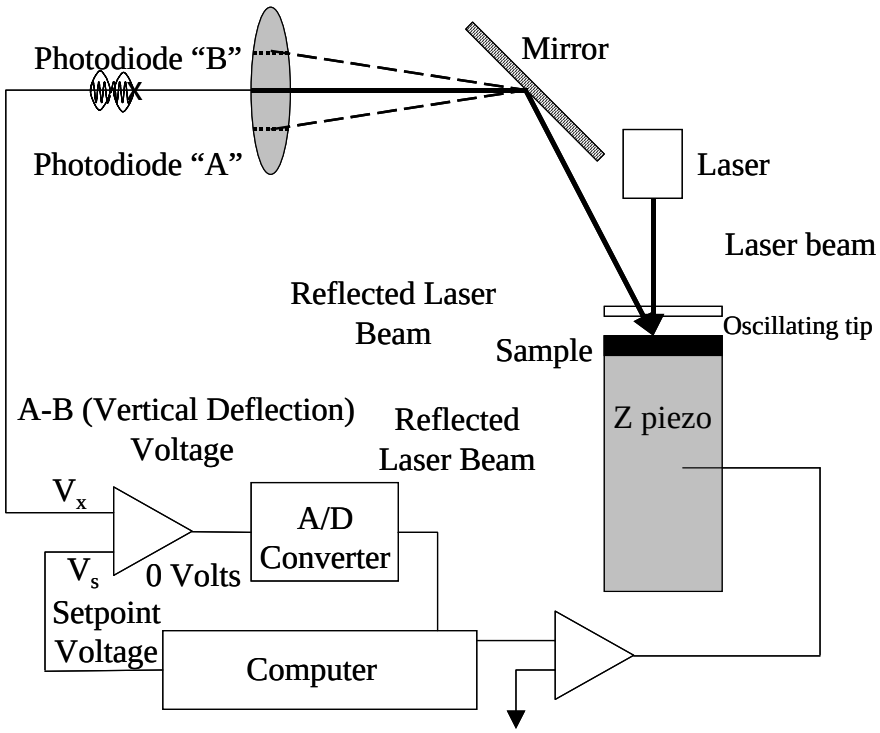

Fig.2.9 Principle of AFM

2.2.3 X-ray Photoelectron Spectroscopy (XPS)

Chemical state of a few nm surface layers is analyzed by X-ray Photoelectron Spectroscopy (XPS) as shown in Fig.2.10. An electron is emitted by the photoelectric effect when homogeneous light is applied material. The measuring method of electron energy and intensity distribution is called XPS method.

$$E_{kin}{}^{v} = h\nu - E_b - \phi$$

where $E_{kin}{}^{v}$, hν, E_b and ϕ are kinetic energy of liberated photoelectron, incident X-ray energy, binding energy of emitted electron for sample and work function for sample. If hν is constant, binding energy can be obtain by measuring the kinetic energy of emitted electron. Identification of element is easily possible by measuring E_{kin} because binding energy of each electron orbit is different. On the other hand, binding energy of same orbit of same element is changed a little by an atomic surrounding state and environment. State analysis of element is possible by measuring this change variation called chemical shift.

Additionally, mean free path of electron is not so long because of scattering and absorption process of electron in solid. Therefore, since XPS method can observe only the surface of nm order, it is suitable for thin film evaluation.

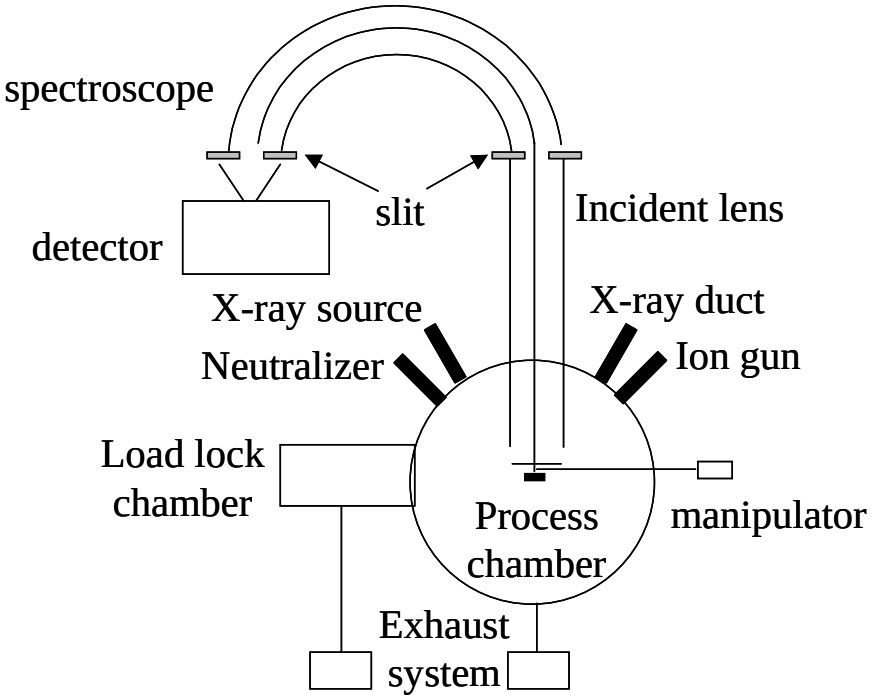

Fig.2.10 Schematic of XPS system

2.2.4 Reflection High-Energy Electron Diffraction (RHEED)

An electron beam is suitable for observing surface structure because of large interaction with an atomic. Reflection High-Energy Electron Diffraction (RHEED) as shown in Fig.2.11 is method to investigating the crystallography of sample surface by projecting scattered electron beam at surface crystalline lattice on fluorescent screen. 1 to 100-keV electrons are incident on the sample, but because such energetic electrons penetrate deeply, they are made to strike the sample at a shallow, glancing angle of typically 1~3^{o}.

Pattern is changed shape of streak if grain is small and emitted angle of electron beam is not large in order to extend vertically spot in inverse proportion to the domain width of a flat film. In other words, pattern is shape of streak if a 2-dimensional crystal is small (narrow flat region), and pattern is punctiform if a 2-dimensional crystal is large (wide flat region).

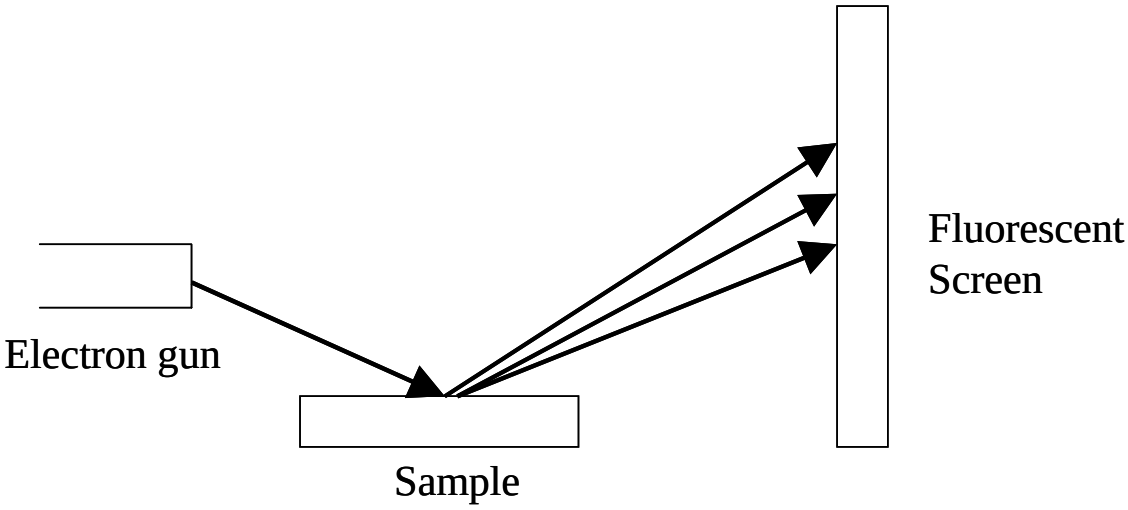

Fig2.11 Schematic of RHEED system

2.2.5 Secondary Ion Mass Spectrometry (SIMS)

Depth profile, composition analysis of element and surface analysis of the sample is evaluated by Secondary Ion Mass Spectrometry (SIMS) as shown in Fig. This technique is element specific and is capable of detecting all elements as well as isotopes and molecular species. The basis of SIMS, shown in Fig.2.12, is the destructive removal of material from the sample by sputtering and the analysis of that material by a mass spectrometer. A primary ion beam (Ar^+, O_2^+, Cs^+ and etc.) impinges on the sample, and atoms from the sample are sputtered or ejected from sample.

Measurement by SIMS is explained in more detail under tri-level as follows;

(1) A primary ion beam with 200 eV~20 keV is irradiated to a solid sample, and secondary ion and neutral particle are emitted from surface monolayers of a sample by sputtering phenomenon with an electron, X-rays and reflective ion.

(2) Mass of positive or negative secondary ion is separated.

(3) An elemental analysis for 2-dimention or 3-dimention of a sample is carried out by measuring intensity due to correcting separated secondary ion or by observing image.

Electronegative oxygen (O_2^+) is a secondary ion yield-enhancing species for electropositive elements (e.g., B and Al in Si) which produce predominantly positive secondary ions. The situation is reversed for electronegative elements (e.g., P, As and Sb in Si), having greater yields when sputtered with electropositive ions like cesium (Cs^+).

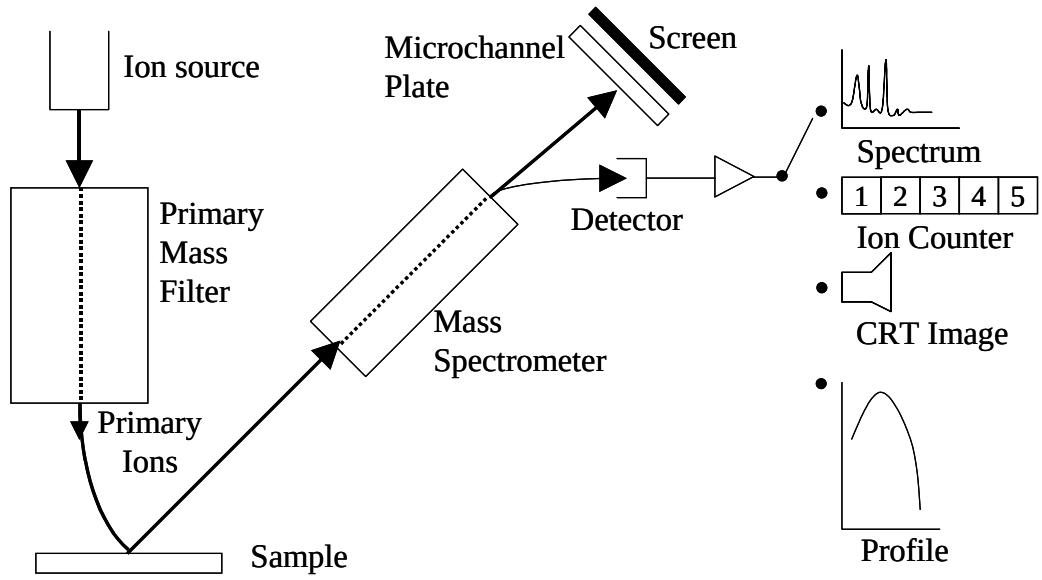

Fig.2.12 SIMS schematic

2.2.6 Four-Point Probe

The four-point probe technique using four-probe is one of the most common methods for measuring the semiconductor resistivity because two-point probe methods are more difficult to interpret. This technique is calculated resistance by applying the current between outside 2 terminals (between A probe and D probe) and by measuring potential difference between inside 2 terminals (between B probe and C probe) as shown in Fig.2.13 The resistance by two-probe technique is higher than accurate resistance by including the contact resistance (R_c) at metal probe/semiconductor contact and spreading resistance (R_{sp}) under each probe. Nether R_c nor R_{sp} can be accurately calculated so that semiconductor resistance (R_s) cannot be accurately extracted from the measured resistance. On the other hands, four-probe technique can be neglected those parasitic resistances because the current value which flows between terminals is very small, and so potential drop can be disregarded. In this study, sheet resistance is measured by four-probe technique.

For an arbitrarily shaped sample the sheet resistance (ρ_{sh}) is given by

$$\rho_{sh} = \frac{V}{I} \times CF$$

where CF is correction factor that depends on the sample geometry. If distance between probes (s; in this study, s=1 mm) is very shorter than width of a sample (d), CF equals to $\pi/\ln(2)=4.54$.

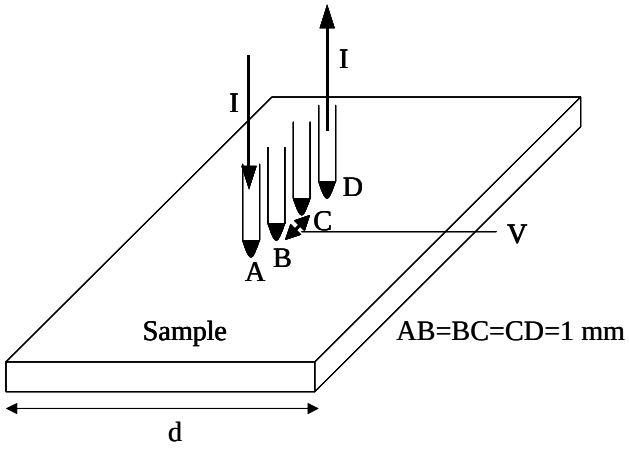

Fig.2.13 A collinear four-point probe

2.2.7 Spectro Ellipsometry (SE)

Ellipsometry as shown in Fig.2.14 is used predominantly to measure the thickness of thin dielectric films on highly absorbing substrates but can also be used to determine the optical constants of films or substrates by measuring the state of polarization of polarized light. When light is irradiated at a material, the state of polarization is different from incident light and reflected light. The state of reflected surface is measured by that difference.

The incident polarized light can be resolved into a component p, parallel to the plane of incidence and a component s perpendicular to the plane of incidence. The two components experience different amplitudes and phase shifts upon reflection from absorbing materials and for multiple reflections in a thin layer between air and the substrate. The complex reflection ratio ρ defined in terms of the reflection coefficients R_p and R_s or the ellipsometric angles Ψ and Δ

$$\rho = \frac{R_p}{R_s} = \tan(\Psi)^{j\Delta}$$

is measurable.

Ψ and Δ determine the differential changes in amplitude and phase, respectively, experience upon reflection by the component vibrations of the electric field vectors parallel and perpendicular to the plane of incidence. Since Ψ and Δ are function of complex index of reflection, film thickness, incident angle and measured wavelength, film thickness can be calculated from the results of ellipso parameter.

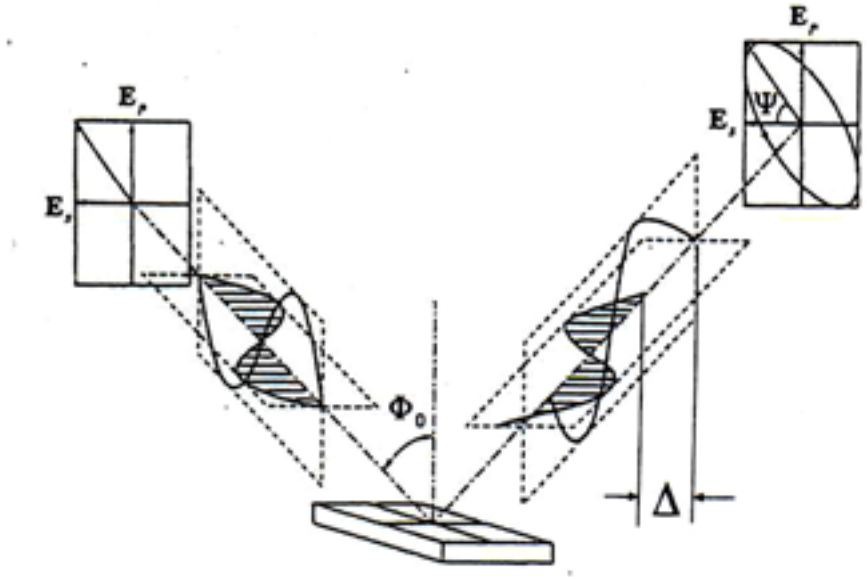

Fig.2.14 Spectro Ellipsometry schematic

2.2.3 Transmission Electron Microscopy (TEM)

Cross section of the sample is observed by Transmission Electron Microscope (TEM). TEM is microscopic equipment for observing internal structure of a thin sample by radiating electron beam to it.

Fig.2.15 shows schematic cross section of a TEM. The principle of TEM is similar to that of optical microscope. In case of TEM, observation is made in a high vacuum, and an electron gun and electromagnetic lenses are used in place of a light source and optical lenses, respectively. Because wavelength of electron beam is less than that of visible ray, resolution of TEM is higher than that of optical microscope.

The thickness of sample must be not greater than 0.1 μm so as to transmit electron beam.

In some case, focused Ion Beam (FIB) equipment is used for the lamination of the sample.

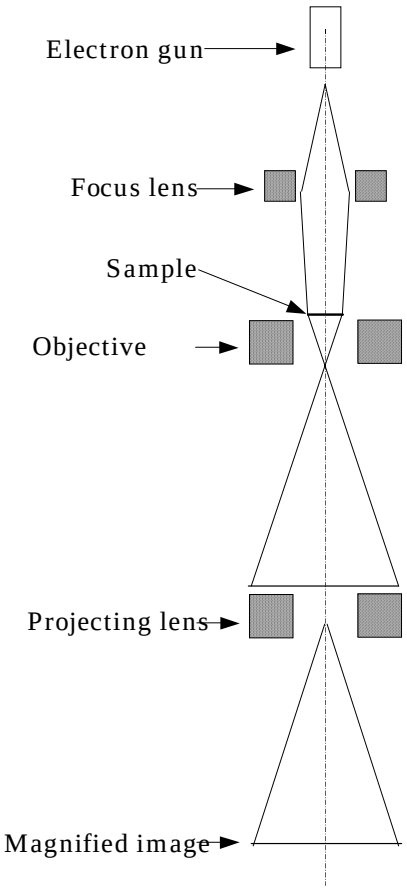

Fig.2.15 schematic cross section of a TEM

Chapter3

Fabrication and Characterization of MIS Capacitors

3.1 Introduction

In this sub section, the fabrication process and characterization for MIS capacitors is discussed.

3.2 Fabrication of Al/High-k/n-Si(100) MIS Capacitors

Figure 3.1 shows outline of fabrication process of Al/Oxide (high-k thin films) /n-Si(100) MIS capacitors. First, high-k thin films were deposited of chemically cleaned and HF dipped n-Si(100) substrates by using ultra high vacuum molecular beam deposition (MBD) system equipped with electron beam evaporators. The pressure during deposition was 10^{-9} to 10^{-7} Torr. The deposition temperature was R.T~250^{o}C. The deposited films were subsequently annealed by RTA system at 600^{o}C in N_2 for 5min. Then, the moisture absorption test was carried out. In this study, the tests before and after Al gate electrode formation were carried out. Electrical characteristics (C-V, J-V), AFM and XPS measurements were performed to investigate the stability of the films.

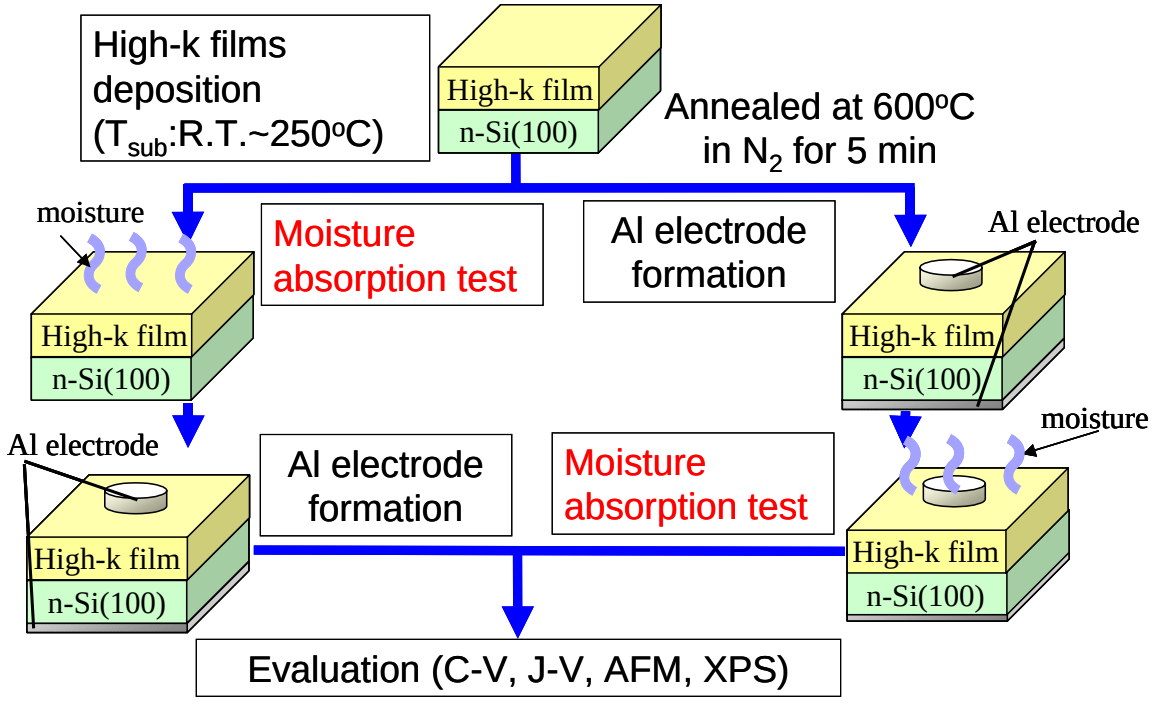

Fig.3.1 Experimental procedure

3.3 Characterization of Al/High-k/n-Si(100) MIS Capacitors

3.3.1 Absorption Test in acryl apparatus

Acryl (PMMA) apparatus is generally used as preservation desiccators. It is suggested that rare earth oxide films is degraded by the effect of CO_2 gas from acryl apparatus. And so, in order to investigate the effect of desorption gas from acryl apparatus, the test was carried out using various high-k materials, such as rare earth oxide (La_2O_3, Pr_2O_3, Sm_2O_3, Eu_2O_3, Gd_2O_3, Dy_2O_3, Yb_2O_3, and Lu_2O_3), ZrO_2 and SiO_2 used conventionally. Figure 3.2 shows change of CET, leakage current density, surface roughness and correlation between the degradation of leakage current density and film roughness for various films. In case of SiO_2, no degradation was observed, indicating very good stability. On the other hand, all high-k films, even ZrO_2, had significant degradation of electrical characteristics, and surface after the tests became rough for the samples without Al electrode. However, the degradations change significantly in deferent oxides. The degradations of Yb_2O_3 and Gd_2O_3 films were significantly smaller than those of other rare earth oxides. In generally, it is thought that Lu_2O_3 is good stability in moisture ambience due to the biggest lattice energy, in other words, strongest combination in rare earth oxides. According to experimental results, however, the change of leakage current was small, but that of CET is very large. Figure 3.2 (e) shows the correlation between the degradations of leakage current and film roughness. It should be noted that the leakage current increased with the increase of roughness. The increase factor of leakage current is caused by surface roughness.

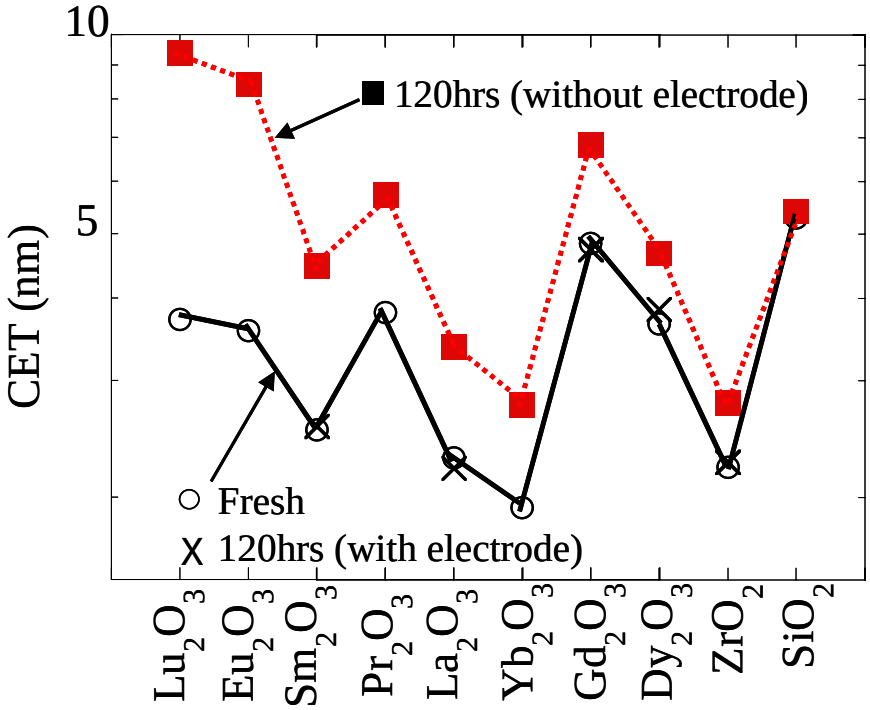

Fig.3.2 (a) Change of CET for all studied.

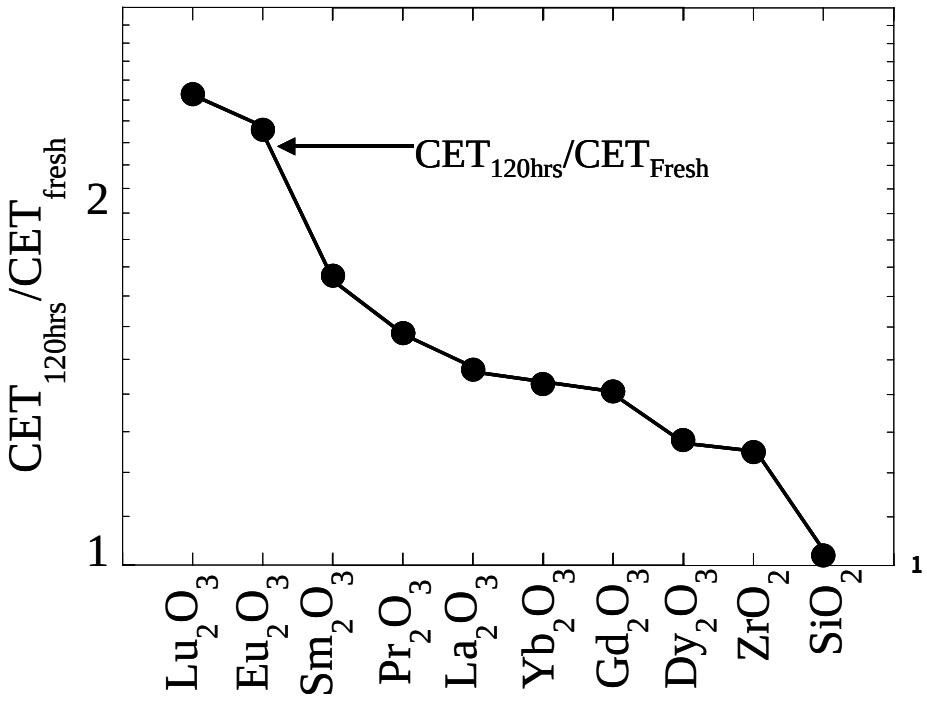

Fig.3.2 (b) Change of CET_{120hrs}/CET_{Fresh} for all studied

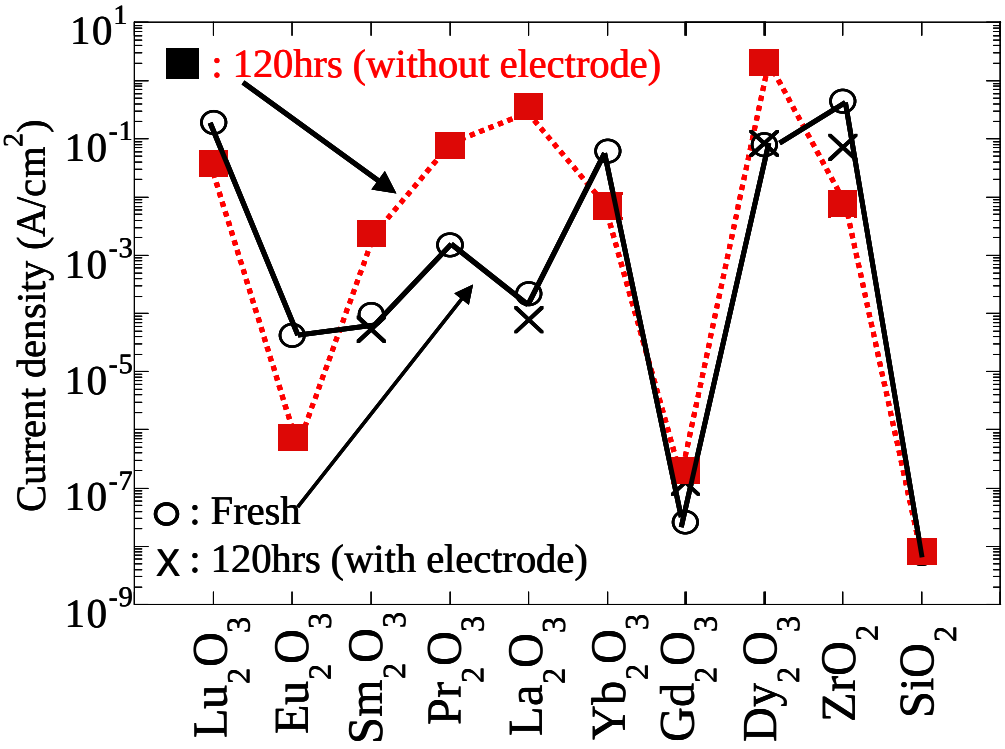

Fig.3.2 (c) Change of leakage current @ +1V for all studied

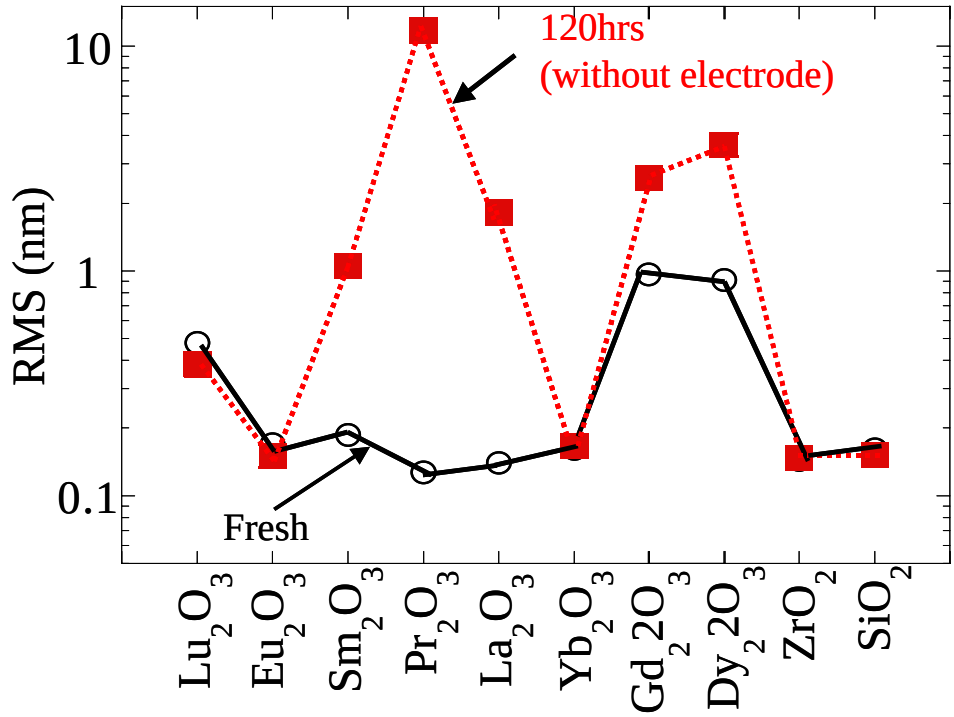

Fig.3.2 (d) Change of RMS for all studied.

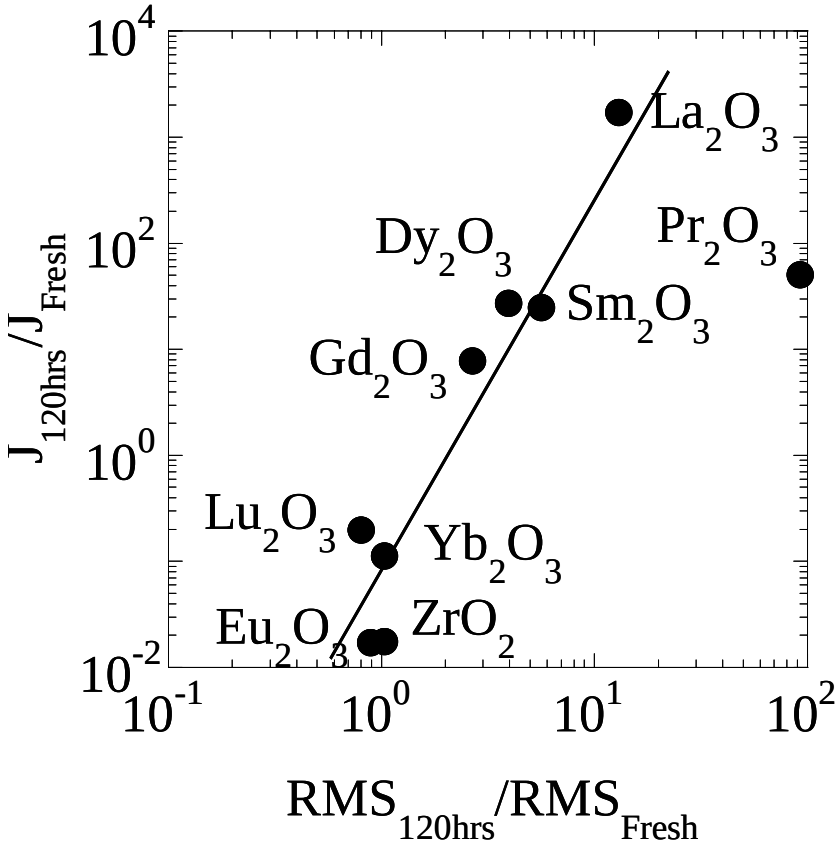

Fig.3.2 (e) Change of J_{120hrs}/J_{fresh} vs. RMS_{120hrs}/RMS_{Fresh} for all studied.

C-V characteristics for SiO_2, ZrO_2, Yb_2O_3, Sm_2O_3 are shown in Fig.3.3. A solid line shows a sample without tests, and a broken line shows a sample after the tests in case of using acryl (PMMA) apparatus for 120 hours. Measurement frequency is 100 kHz. C-V characteristic for SiO_2 was no change. On the other hands, the accumulation capacitance of ZrO_2 was significantly decreased similarly to that of rare earth oxides. Increasing amount of CET for ZrO_2, Yb_2O_3 and Sm_2O_3 are 25, 43 were 77 %, respectively. CET for almost all others studied materials was increased.

Figure 3.4 shows the change of J-V characteristics of SiO2, ZrO2, Yb2O3 and Sm_2O_3, respectively. In the case of Sm2O3, the leakage current density @+1V increased after the test. In general, the moisture-absorbed thicker film is expected to have smaller leakage current. However, when the roughness of the film increases, the leakage current is expected to increase.

Fig.3.5 shows the typical AFM images of SiO_2, ZrO_2, Yb_2O_3 and Sm_2O_3 films before and after the tests. The surface roughness of SiO_2, ZrO_2 and Yb_2O_3 changed a little, while that of Sm_2O_3 became dramatically large.

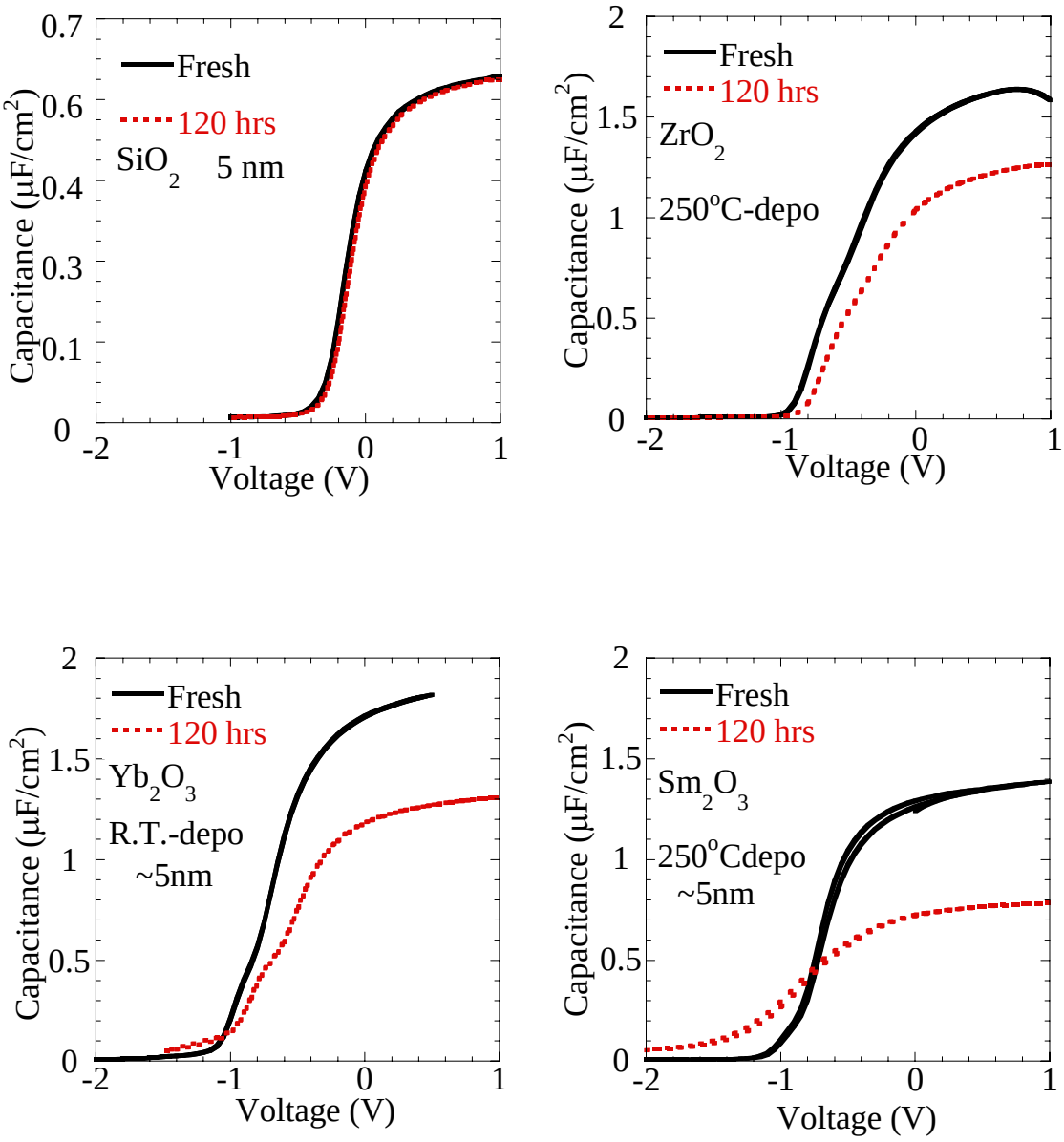

Fig. 3.3 Change of C-V curves for (a) SiO_2, (b) ZrO_2, (c) Yb_2O_3 and (d) Sm_2O_3

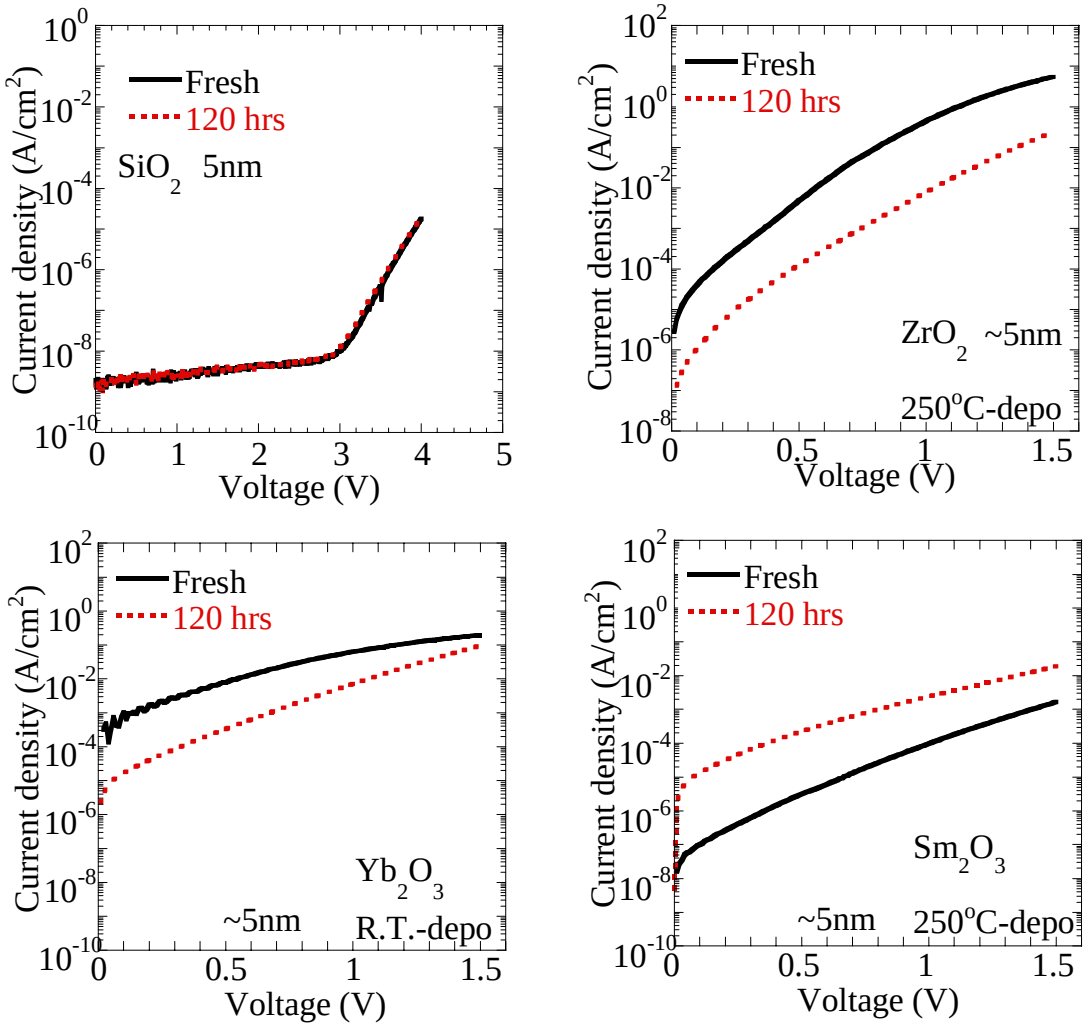

Fig.3.4 Change of J-V curves for (a) SiO_2, (b) ZrO_2, (c) Yb_2O_3 and (d) Sm_2O_3.

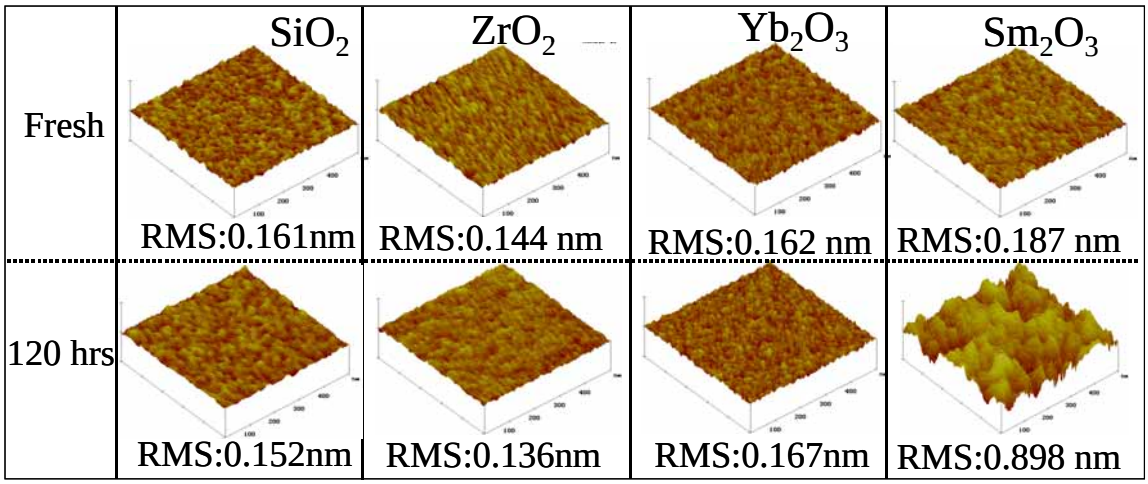

Fig. 3.5 Change of RMS for (a) SiO_2, (b) ZrO_2, (c) Yb_2O_3 and (d) Sm_2O_3

3.3.2 The effect of desorption gas from the apparatus

In order to clarify the effect of desorption gas from the apparatus, the moisture tests were carried out in acryl and glass apparatus. Figure 3.6 and Fig.3.7 show the change of electrical characteristics (C-V and J-V) and AFM images for Pr_2O_3 after 24 hours test. Though the film was degraded in case of using glass apparatus, the degradation was larger in case of using acryl apparatus from C-V characteristic. However, changes of leakage current and RMS were a little from J-V characteristic and AFM image in case of using glass apparatus.

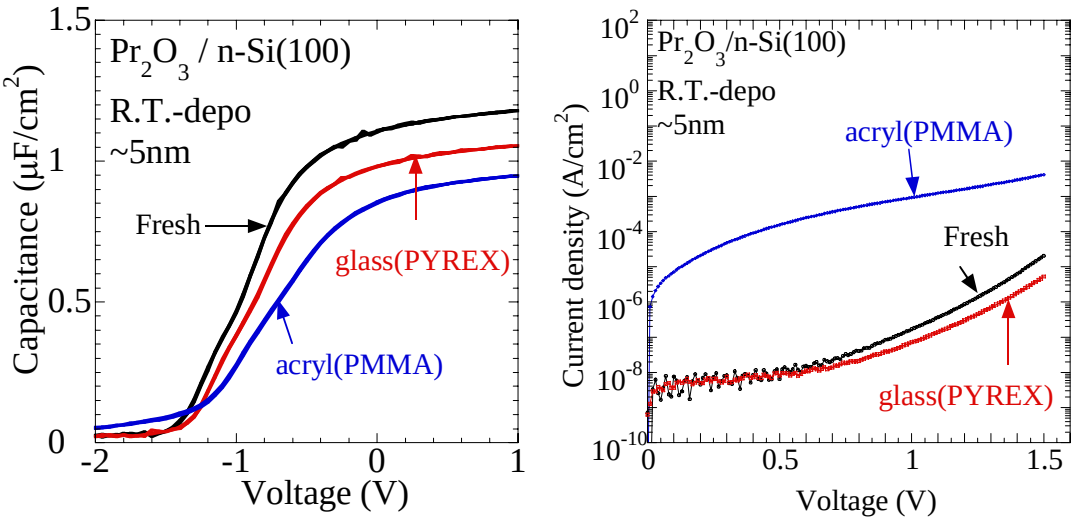

Fig.3.6 Change of electrical characteristics (C-V and J-V) for Pr_2O_3 at deferent experimental apparatus

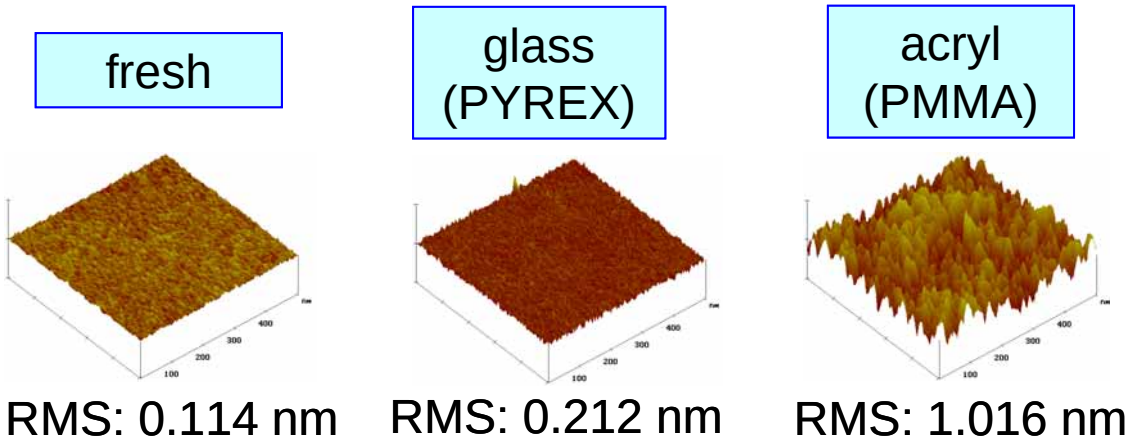

Fig.3.7 Change of RMS for Pr_2O_3 at deferent experimental apparatus

Various hydrocarbons were dissolved from the acryl apparatus from TDS (Thermal Desorption Spectroscopy) measurement as shown Fig. 3.8. The hydrocarbon was considered to be absorbed into the deposited films, and degraded the film quality.

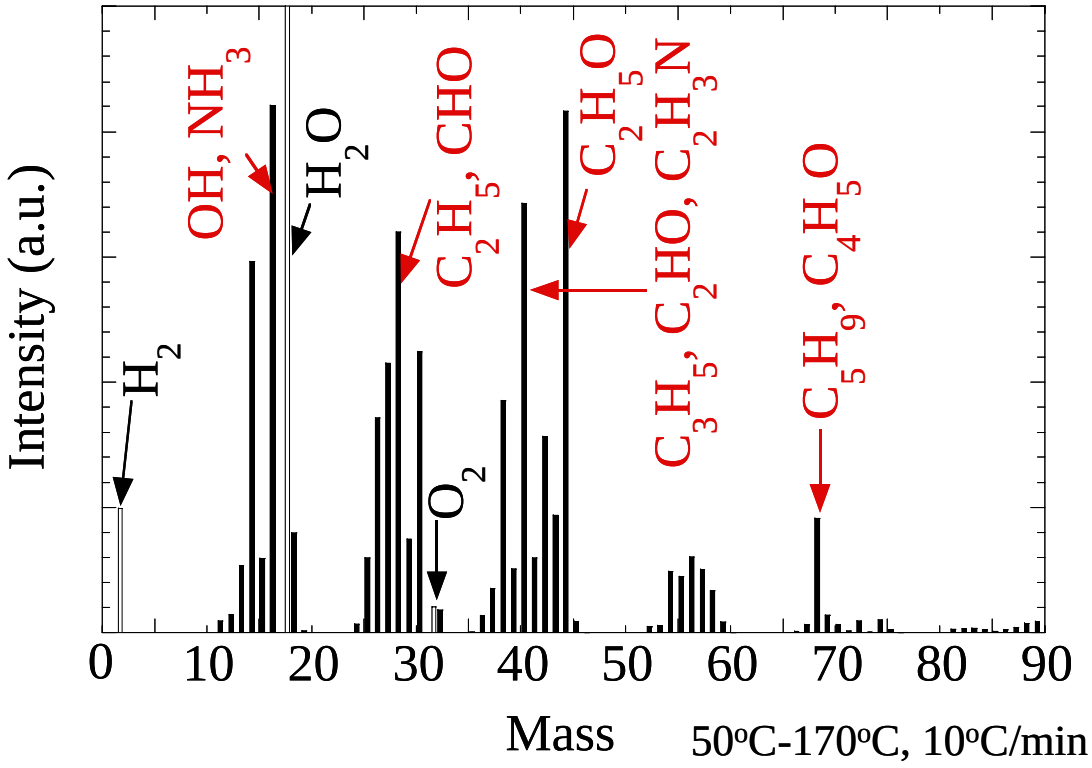

Fig.3.8 TDS spectra for acryl experimental apparatus

Figure 3.9 shows Pr3d and O1s spectra in XPS (X-ray Photoelectron Spectroscopy) at standard take-off angle ($\theta=45^{o}$). From Pr3d spectra in XPS results, there was large decrease of Pr-O spectra in case of using acryl apparatus. From O1s spectra in XPS results, oxide peak was little and signal of strong peak due to C=O combination in around 531.7eV was observed in case of using acryl apparatus.

Figure 3.10 shows the XPS depth profiles of Pr3d and O1s spectra by varying take-off angle. From these XPS signals, it was found that Pr peak increased with the increase of take-off angle. This suggests that the CO contamination layer without Pr was deposited on the film surface. Besides, the chemical shifts of Pr-O and C=O peak were observed. This may be caused by the CO.

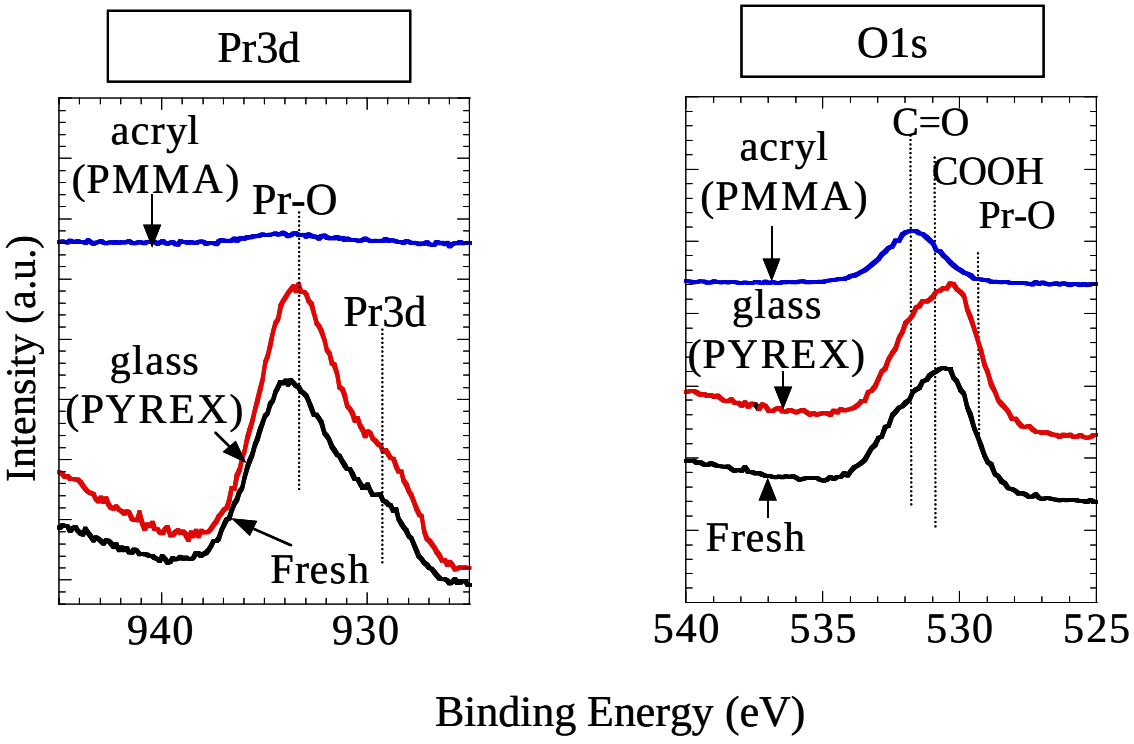

Fig.3.9 Pr3d and O1s spectra before and after the tests at standard take-off angle (45^{o})

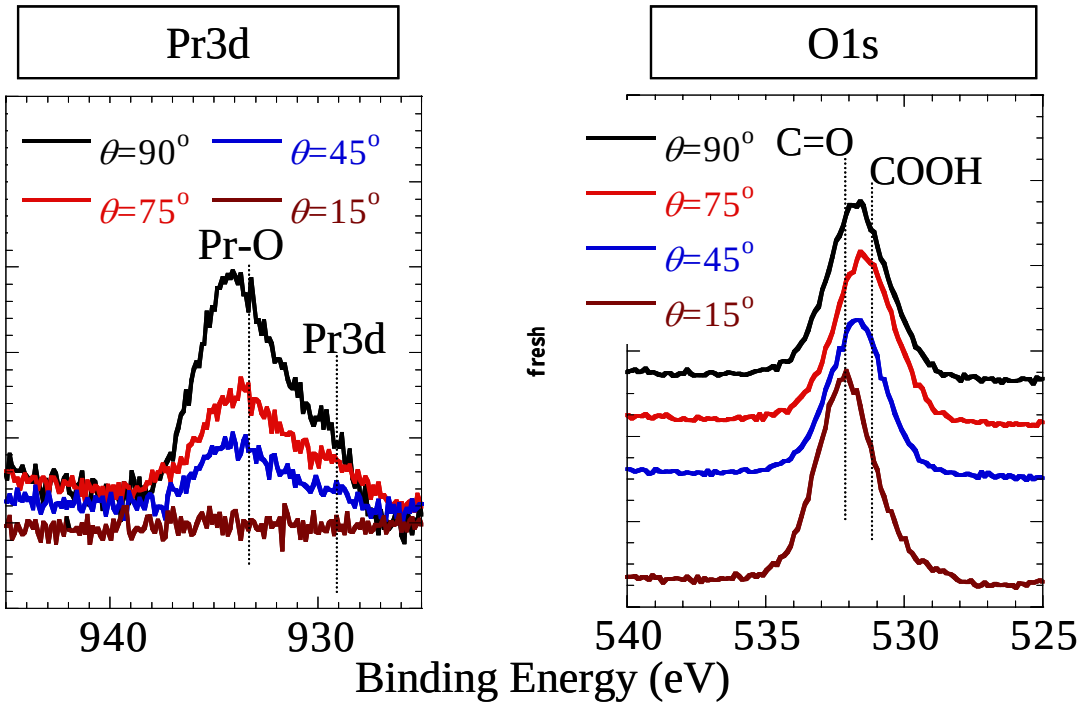

Fig3.10 Pr3d and O1s XPS spectra by varying take-off angle in case of using acryl apparatus

3.3.3 The effect of post annealing

In order to clarify the effect of post annealing whether H_2O in films vapor and film quality is recovered, the post annealing tests were carried out. Samples were used after the test in case of using glass apparatus for 24 hours. Post annealing was carried out by RTA system at 200°C in N_2 for 5 minutes. Figure 3.11 shows the change of electrical characteristics (C-V and J-V) after annealing. Black line is fresh, red line is after the test in casing glass apparatus, and blue line is after the annealing called post annealing. Though the accumulation capacitance of sample after post annealing increase a little, not be completely recovered. In this study, it was found that the perfect improvement of film quality was not obtained similarly from J-V curve.

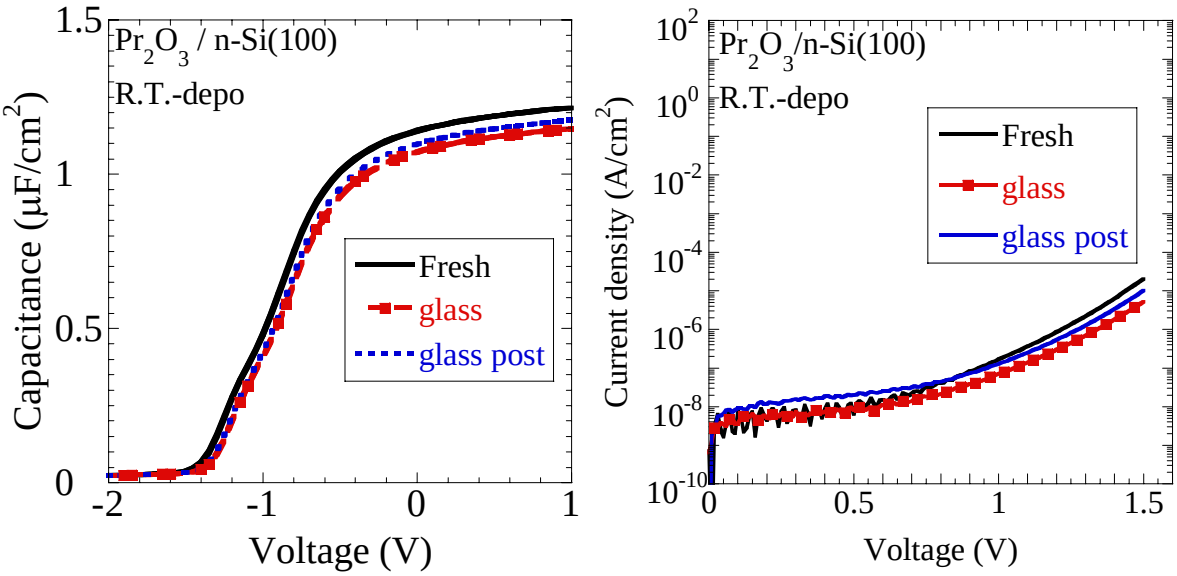

Fig.3.11 Change of electrical characteristics (C-V and J-V) after post annealing

3.3.4 The effect of Al gate electrode coverage

The moisture absorption test in case of using acryl apparatus after Al gate electrode was carried out. In Fig.3.12, C-V characteristic of before and after the test was shown. There was little degradation observed even after 24 hours test. It was found that the degradation was completely suppressed by gate electrode coverage.

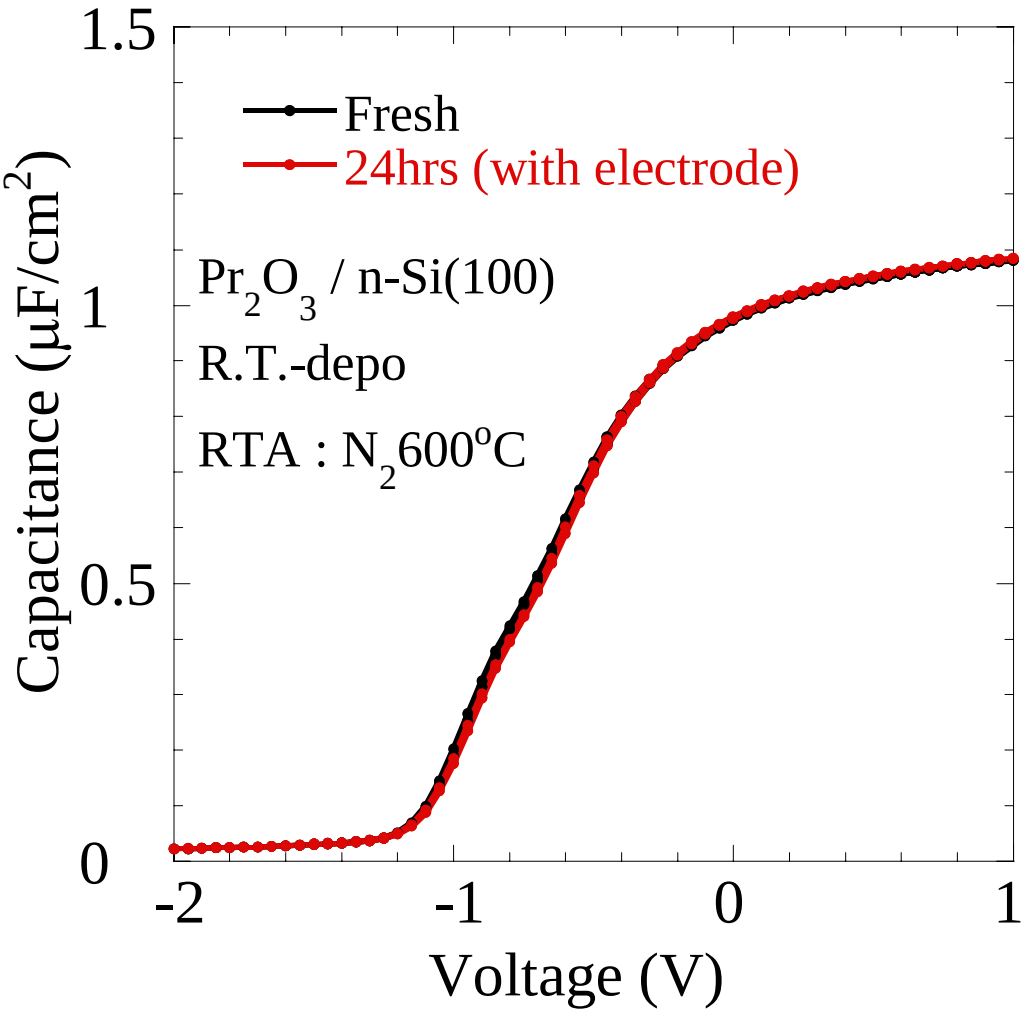

Fig.3.12 C-V curves for Pr_2O_3 before and after the Al electrode formation

3.4 Summary of this chapter

The moisture absorption tests for high-k thin films were carried out in case of using acryl and glass apparatus. Though the film was degraded in case of using glass apparatus, the degradation was larger in case of using acryl apparatus. Especially, for J-V characteristics and roughness of the film surface, this phenomenon was observed. It is suggested that rare earth oxides became hydroxide and carbonate in case of using glass and acryl apparatus, respectively. And so not only rare earth metal oxides but also ZrO_2 was degraded in moisture ambience.

Various hydrocarbons were dissolved from the acryl apparatus from TDS measurement. Therefore, the hydrocarbon was considered to be absorbed into the deposited films, and degraded the film quality.

There was decrease of Pr-O peak was little and signal of strong peak due to C=O contamination in around 531.7 eV from XPS measurement. It is suggested that there is a possibility that entire rare earth oxide was carbonated.

As a result of the effect of post annealing, though the accumulation capacitance of sample after post annealing increase a little, not be completely recovered.

It was confirmed that the degradation was completely suppressed by gate electrode coverage. The hygroscopic problem of the high-k films could be solved by the gate electrode coverage. However, long-term reliability test in electrical characteristics is necessary.

Chapter4

Investigation of Boron Absorption and Penetration by Plasma Doping Method

4.1 Introduction

In this sub section, the fabrication process and characterization of for Plasma Immersion Ion Implantation (PIII) is discussed.

4.2 Broad flow chart of experimental procedure

Figure 4.1 shows outline of fabrication process of ultra-shallow junction. First, boron for p-Si formation was doped on HF dipped Hydrogen-terminated n-Si(100) substrate with a resistivity of 8-12 (Ω-cm) by using Plasma Doping (PD) system with Plasma Immersion Ion Implantation (PIII) technique. Therewith, plasma characteristics were measured by Langmuir probe technique. The pressure during doping was 10^{-1} to 2.5 Pa. The doping temperature was Room Temperature (R.T.). Some as doped samples were measured depth profiles and Concentration of boron by SIMS. Other samples were subsequently annealed by RTA system at 1100°C in N_2 for 3min. Then, the growing thermal oxide (SiO_2) by annealing was removed by HF dipped because measuring resistance was prevented from SiO_2. Finally, sheet resistance was measured by four-point probe technique.

Additionally, explanation about boron implantation by PD or Gas phase Doping (GD) is given a full account in sub-section of section 4.3. Then, relation between bias power and bias voltage, and plasma characteristics is given a full account in appendix A and appendix B, respectively.

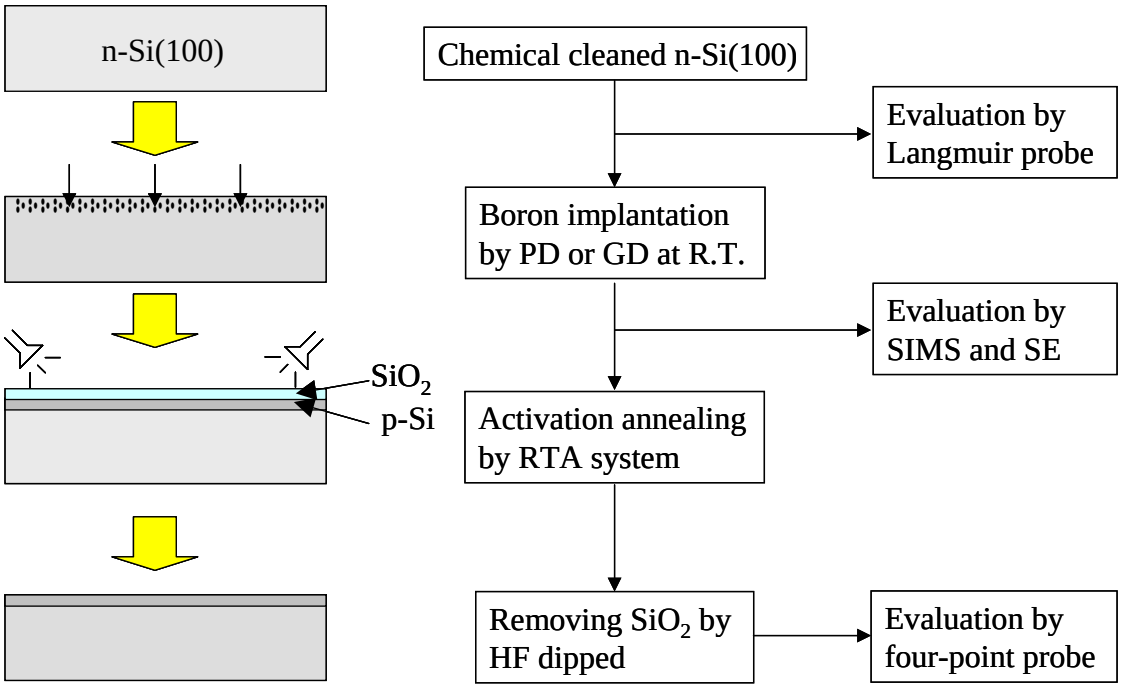

Fig.4.1 Experimental procedure

4.3 Mechanism of boron absorption and penetration

4.3.1 First approaches

Fabrication procedure

Figure 4.2 shows fabrication procedure as first step in plasma doping at R.T. First, He plasma under these conditions, Source Power (S.P.) of 1500 W, flowing rate of 198 sccm for 1 second, was produced after produced Ar plasma under these condition, S.P. of 500 W, flowing rate of 30 sccm for 1 second, and then B_2H_6 gas was introduced, mixing plasma ofB_2H_6 and He under these condition, S. P. of 1500 W, Bias Voltage (B.V.) of –60 V, flowing rate of B_2H_6/He=2/198 sccm for 6seconds. All process was carried out under process pressure of 0.9 Pa and current of electromagnets of 20 A/20 A n PD system.

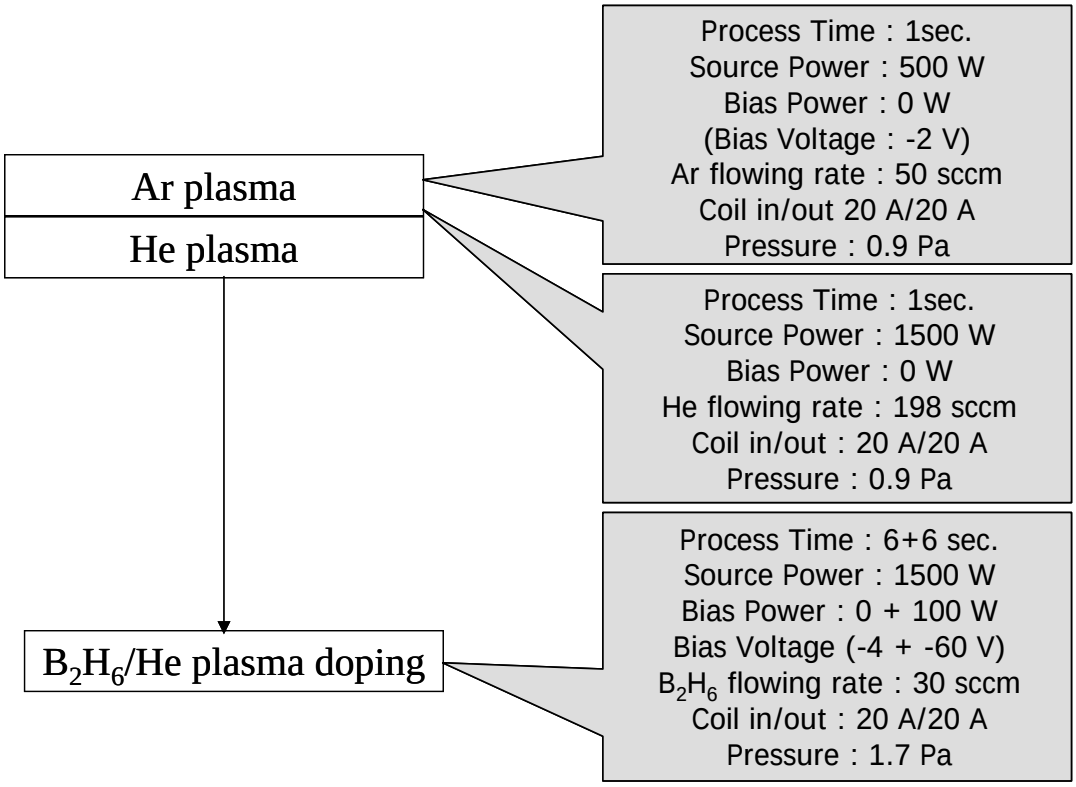

Fig.4.2 Fabrication procedure

Evaluation

The surface of fabricated sample was observed by RHEED as shown in Fig.4.3. Halo pattern of crystal-Si (c-Si) was not observed. It is suggested that surface layer became amorphous by He/B_2H_6 doping. Additionally, cross section TEM observation as shown in Fig.4.4 was carried out in order to confirm whether c-Si became amorphous-Si (a-Si). About 5nm surface layer became a-Si. Therefore, c-Si halo pattern was not observed because surface layer became a-Si. It is suggested that amorphorization coincide with boron doping.

Fig.4.3 Si surface by RHEED observation after do-ping (as-dope)

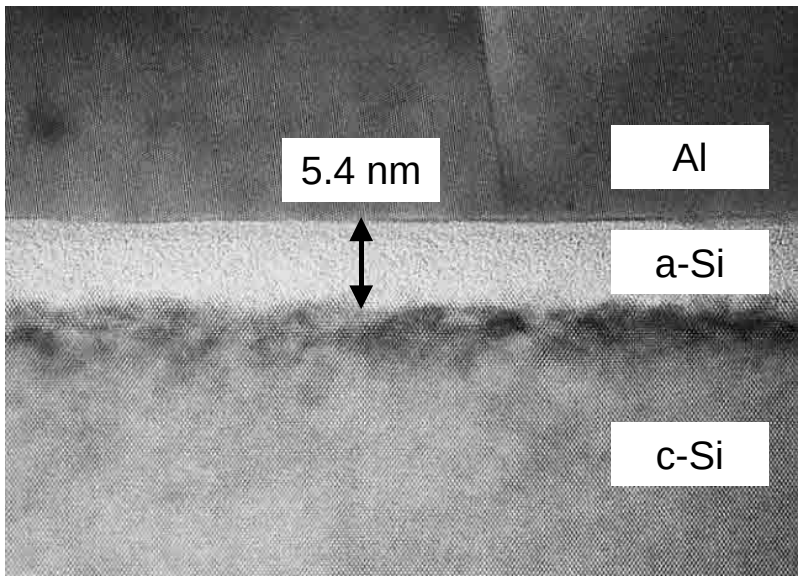

Fig.4.4 Si surface by cross section TEM observation

4.3.2 Boron absorption and penetration

In the vicinity of surface, boron concentration in case of using plasma doping method was strong that of in case of using conventional ion implantation (section 3.4). Therefore, gas phase doping at R.T. was carried out in order to investigate whether boron is absorbed by boron gas flowing only. Additionally, in sub-section 4.3.3, it was confirmed that amorphorization of Si surface was caused by PD. It is indicated that boron penetrates easily into amorphous layer comparing with crystal layer. Therefore, amorphous layer was formed by Ar plasma in order to investigate relation with amorphorization and boron penetration

Fabrication procedure

Figure 4.5 shows fabrication procedure as first step in gas phase doping at R.T. First, two kinds of n-Si(100) substrate with and without Argon plasma treatment were prepared, then B_2H_6 gas was flown on the both samples. These experiences were carried out because it was suggested that absorption of boron was more reacted by exposing of Si connected-hands due to removing native oxide on Si. The thickness of native oxide was about 0.2 nm by SE measurement. Argon plasma treatment was carried out under these conditions that process pressure was 0.7 Pa, gas flowing rate was 50 sccm and bias voltage was –160 V during 70 second. Argon plasma was exited by source power of 1500 W. Meanwhile, B_2H_6 gas of 30 sccm was flown at pressure of 1.7 Pa during 70 seconds. All process of a surface treatment and gas flowing were done at R.T. in PD system.

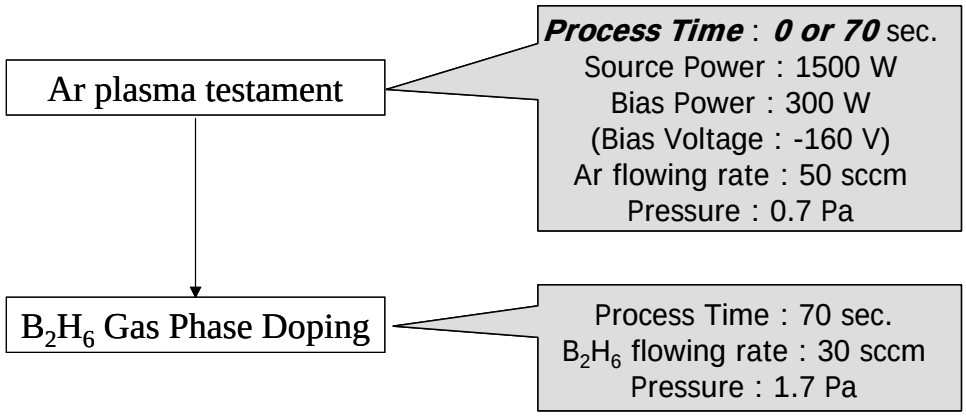

Fig.4.5 Fabrication procedure

Evaluation

Depth profiles and concentration of boron were measured by SIMS as shown in Fig.4.6. The boron dosage of the sample with surface treatment by Argon plasma was 2.8×10^{14} cm^{-2}, on one hand, that of the sample without Ar surface treatment by Argon plasma was 2.0×10^{12} cm^{-2}. The results that the boron dosage of the sample with Ar plasma treatment was two orders of magnitude more than the sample without that were obtained. It is suggested that boron atoms or molecules was absorbed on Si surface by removing native oxide and by activation of Si surface. Thickness of boron penetration was about 5.1 nm and 1.6 nm with and without Ar plasma treatment, respectively. Additionally, knock-on effect by a primary ion was discussed in appendix C.

Figure 4.7 shows AFM images of Si surface (a) with and (b) without Ar plasma treatment. Scan size of x and y were 2μm, respectively and z range was 3nm. The Root Mean Square (RMS) of with and without Argon plasma treatment were 0.142 nm and 0.105 nm, respectively. Good condition of Si surface was obtained.

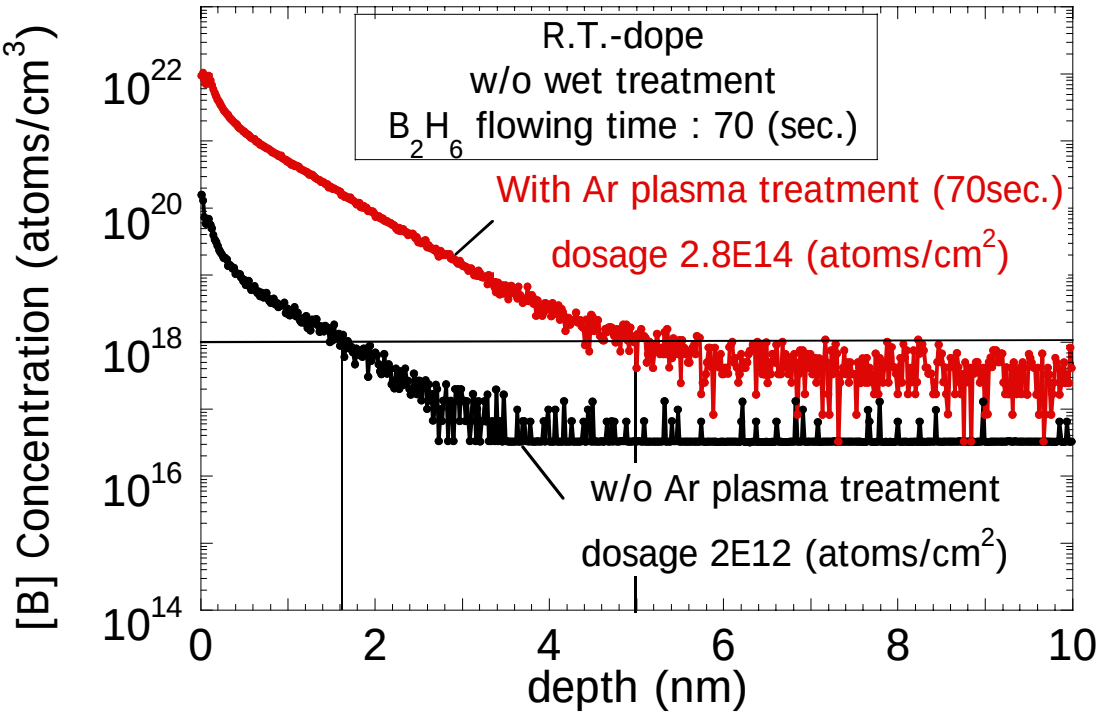

Fig.4.6 Boron depth profiles with and without Argon plasma treatment by SIMS measurement, respectively.

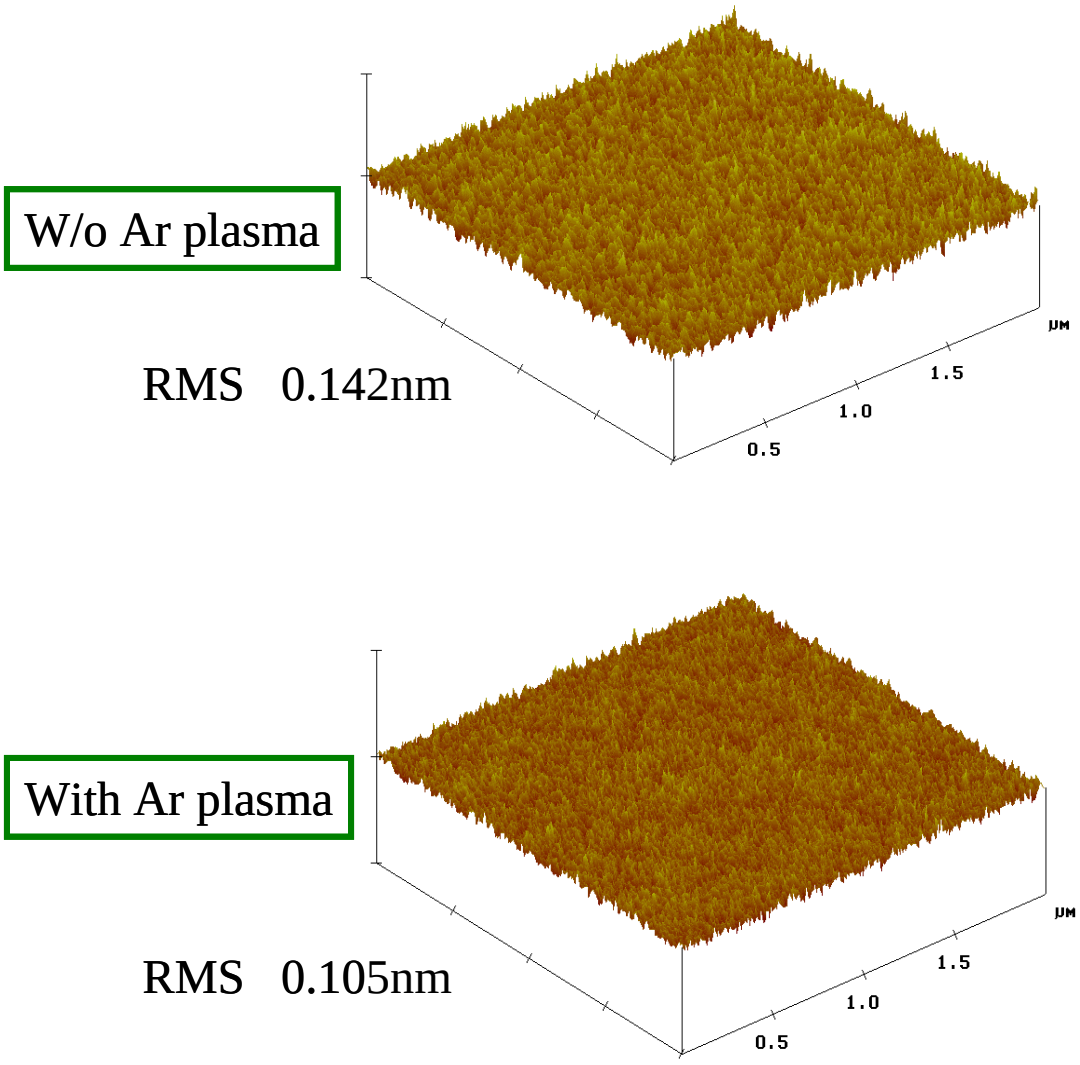

Fig.4.7 AFM images with and without Ar plasma treatment, respectively.

4.3.3 The effect of Argon plasma treatment

In previous sub-section, it was reported that absorption of boron was increased with Ar plasma treatment on Si surface. Therefore, only Ar plasma treatment was performed to investigate the effect of Si surface.

Fabrication

Ar plasma treatment was carried out under the condition that process pressure was 0.7 Pa, gas flowing rate was 50 sccm, and bias voltage was –150 V, respectively as shown in Fig.4.8. Ar plasma was exited by source power of 1500 W. The effect of Ar plasma treatment was investigated by varying process time (0, 6 or 70). Evaluation of effect of that was carried out by RHEED and SE.

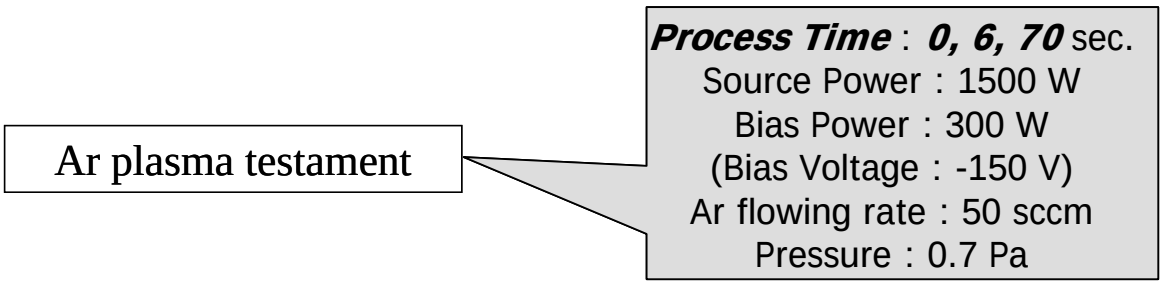

Fig.4.8 Experimental Procedure

Evaluation

The Si surface of the sample with and without Ar plasma treatment was observed by RHEED. The punctiform pattern of Si single crystal in bare Si without Ar plasma treatment was observed as shown in Fig.4.9 (a). On the other hands, that of Si single crystal in the sample with Ar plasma treatment in spite of process time was not observed as shown in Fig4.9 (b) and Fig.4.9 (c). Therefore, it was suggested that 1 nm or more of surface layer became amorphous Si by activation.

The thickness of amorphous layer was measured by SE. First, it was considered double layer structure of native oxide layer/amorphous layer because amorphous Si is

easily reacted to the oxides. The thickness of a native oxide was measured by using the result of the index of reflection which was obtained due to measuring a native oxide of bare Si surface. As a result of measurement, it was estimated that the thickness of amorphous layer during process time of 6 and 70 seconds was about 2.5 nm and 3.5 nm, respectively. Thickness of native oxide was about 0.2~0.3 nm

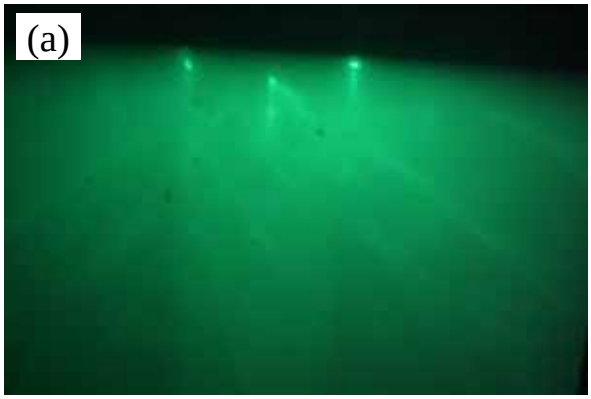

Bare Si without Ar plasma treatment

Ar Plasma treatment during 6 sec. Ar Plasma treatment during 70 sec.

Fig.4.9 Si surface by RHEED observation

4.3.4 Control of boron absorption by process time

Fabrication procedure

It was discussed by varying process time (0, 5, 10, 30 and 70 seconds) of Ar plasma treatment in order to investigate whether boron penetration layer is dependent on amorphous-Si layer. Figure 4.10 shows fabrication procedure. Argon plasma treatment was carried out under the condition that process pressure was 0.7 Pa, gas flowing rate was 50 sccm and bias voltage was –150 V, respectively. Argon plasma was exited by source power of 1500 W. Then, B_2H_6 was flown under the same condition in section 4.3.1.1. Sheet resistance by four-point probe and the thickness of amorphous-Si layer by SE and cross section TEM were performed to investigate this purpose.

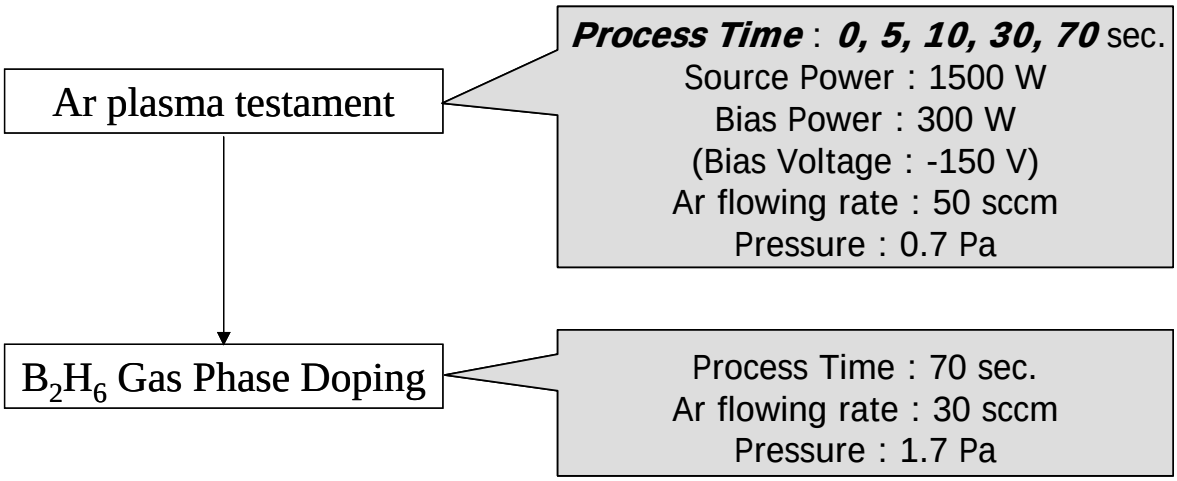

Fig.4.10 Fabrication procedure

Evaluation

Figure 4.11 shows boron depth profile by SIMS for samples with Ar plasma treatment during 0, 5 or 70 seconds, respectively. It was found that dosage of boron was increased with increase Ar plasma treatment time, and boron concentration profile of

two samples with Ar plasma treatment was very similarly in shape for depth of 2.9 nm or more. On the other hand, boron concentration of the sample with Ar plasma treatment for 70 seconds was deeper than that for 5 seconds in depth of 2.9 nm or less. And so, depth of penetrated boron was 4.4, 5.1 nm with Ar plasma treatment time of 5, 70 seconds at 10^{18} cm^{-3}, respectively. Therefore, observation of cross section TEM as shown in Fig.4.12 was carried out to investigation surface state. Fig 4.12 (a) and Fig.4.12 (b) show cross section images of samples with Ar plasma treatment for 5, 70 seconds, respectively. According to Fig.4.12 (a), a-Si of 4.3 nm was grown on Si-substrate, and interfacial layer between a-Si and c-Si was good condition. According to Fig.4.12 (b), however, a-Si of 2.4 nm was grown, interfacial layer of around 3.1 nm between a-Si and c-Si was observed. It is suggested that good interfacial layer was obtained because sputtering of Si-substrate almost never arouse for Ar plasma treatment of 5 seconds, on the other hand, interfacial layer between a-Si and c-Si was obtained damaging layer due to sputtering effect for Ar plasma treatment for 70 seconds. As a result, it is expected that because sufficient bonding-hands of Si were not appeared because oxide layer (SiO_2) layer of a few Å by SIMS and cross-section TEM in case of Ar plasma treatment time of 5 seconds, and so boron concentration of negligible surface layer with Ar plasma treatment for 5 seconds was lighter than that for 70 seconds, on the other hand, boron was gradually penetrated due to existing a-Si or damaging layer.

Sheet resistance of fabrication sample was measured by four-point probe. Figure 4.13 shows relation with sheet resistance and process time of Ar plasma treatment. Sheet resistance of GD only sample (without Ar plasma treatment; 0 sec.) was 342 (Ω/sq.). When re-measurement of GD only sample was carried out after HF dipped for 5 seconds, sheet resistance was 139 (Ω/sq.). It is suggested that this sample equal to bare Si because resistivity of used bare n-Si(100) is 8 (W-cm), in other words, sheet resistance is 135 (Ω/sq.), in this study. It couldn't be not measured by 4-point probe due to lightly concentration of boron. The result was obtained that sheet resistance was increased with Ar plasma treatment time of 5 to 10 seconds, and was decreased with increase Ar plasma treatment time of 10 to 70 seconds. It is suggested that amount of absorption and penetration of boron was increased with increase process time of that because the configuration of B_2H_6 gas flowing was same for all samples, and sheet resistance was increased with Ar plasma treatment time of 5 to 10 seconds because the sample of Ar plasma treatment time of 5 seconds is kept state at n-type Si.

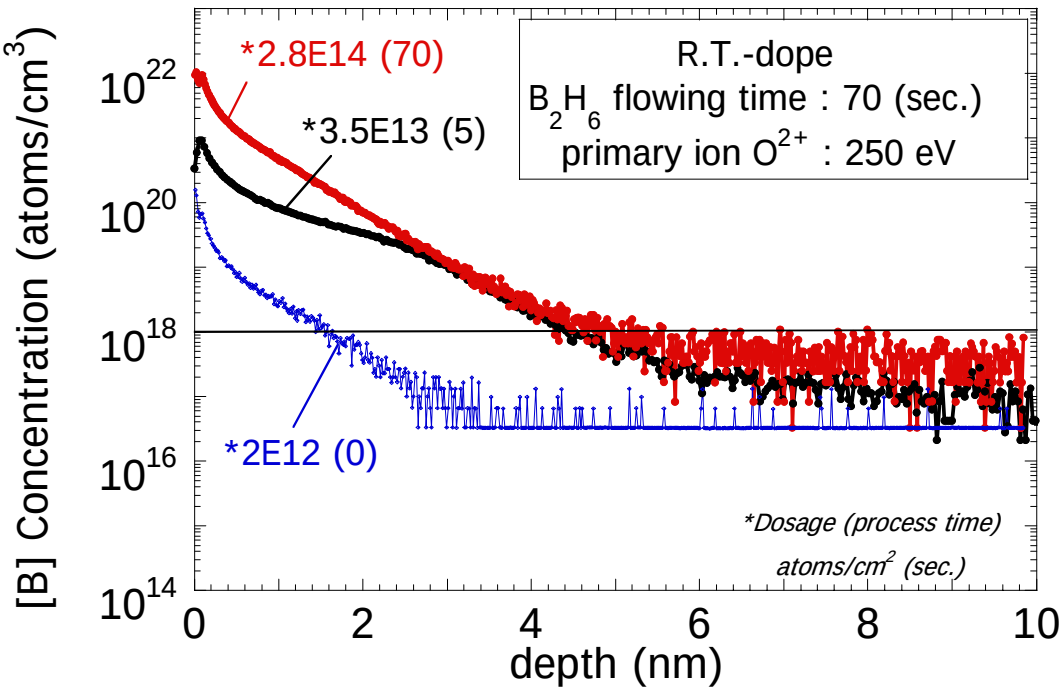

Fig.4.11 Boron depth profile by varying Ar plasma treatment time

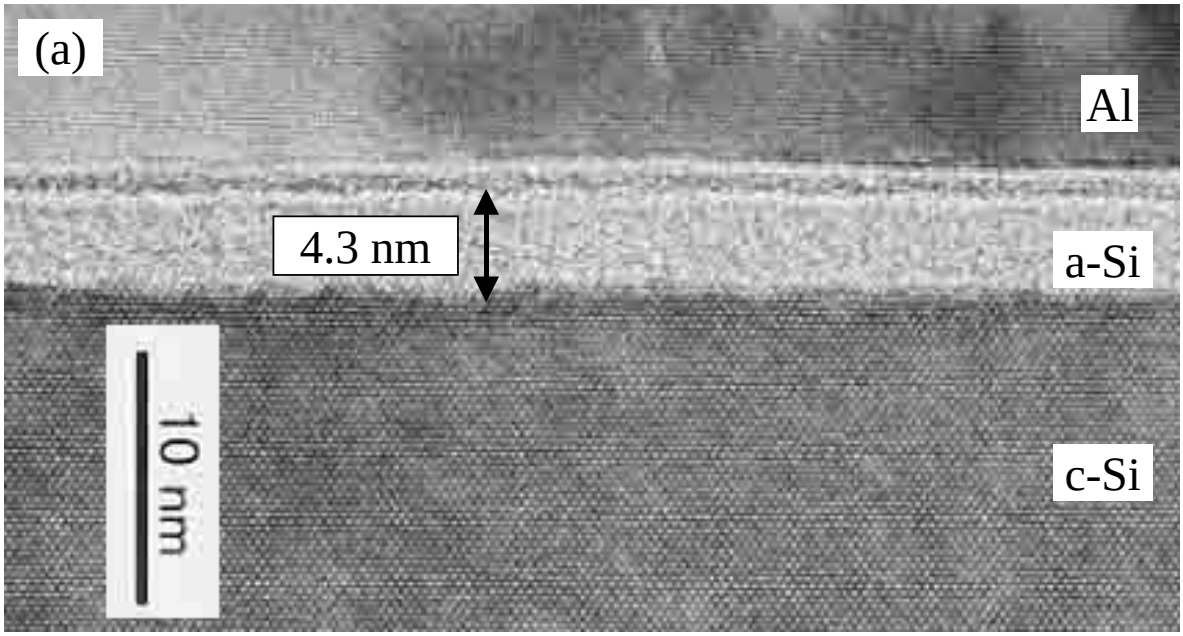

Fig 4.12 (a) cross-section TEM image for Ar plasma treatment time of 5 seconds.

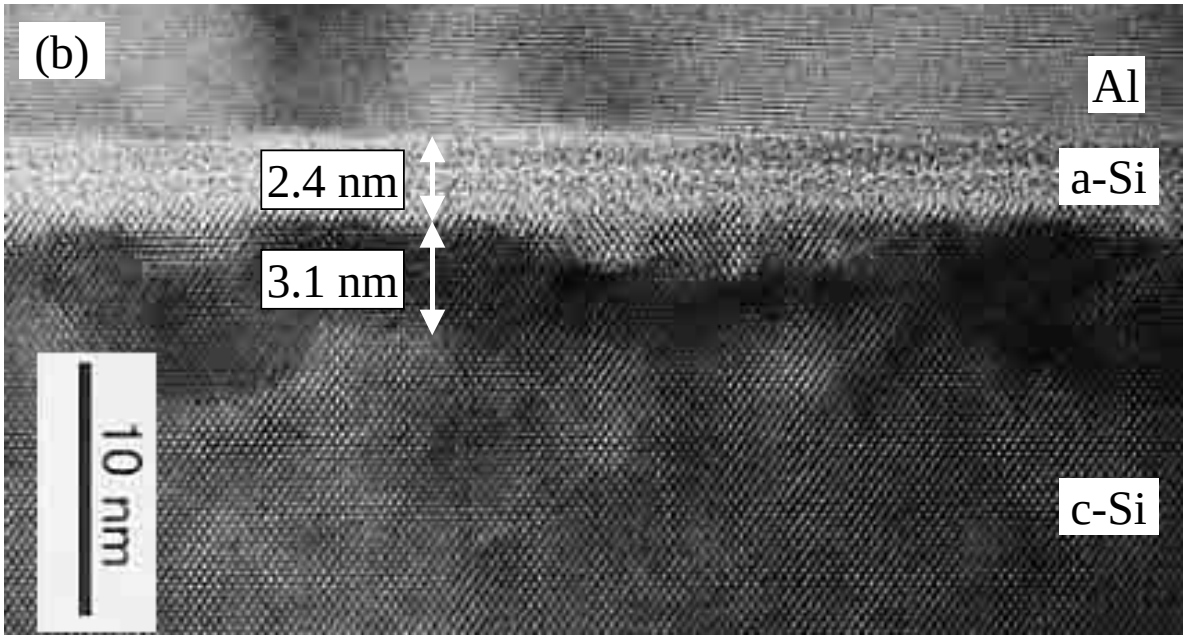

Fig 4.12 (b) cross-section TEM image for Ar plasma treatment time of 70 seconds.

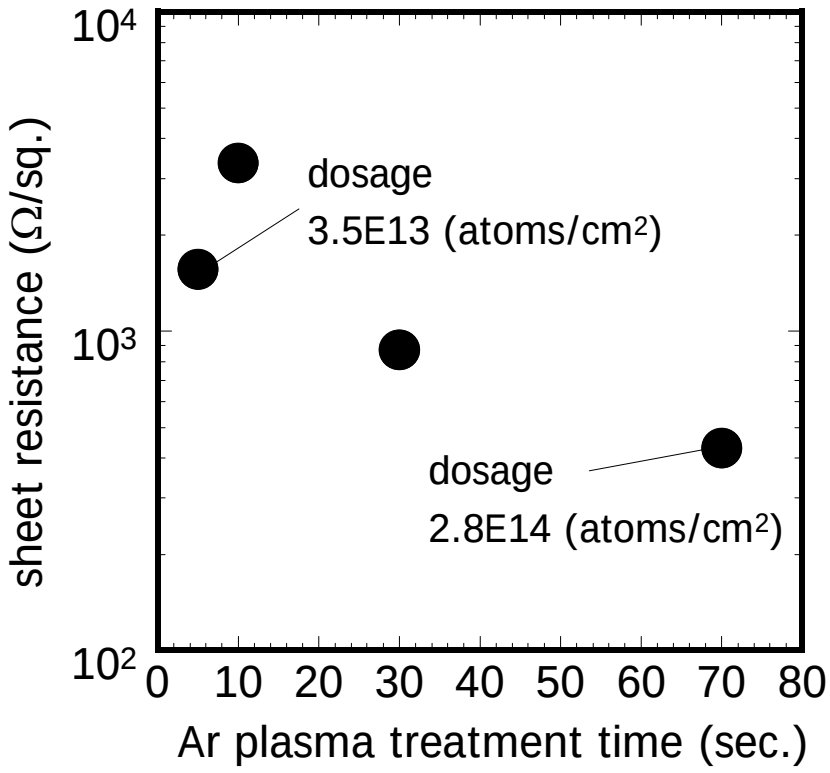

Fig.4.13 Relation with sheet resistance and Ar plasma treatment time

4.3.5Control of boron penetration by bias voltage

Fabrication procedure

It was discussed by varying bias voltage (-70 V, -150 V and –210 V) as another means of control of the thickness of amorphous-Si layer in order to investigate whether boron penetration layer is dependent on amorphous-Si layer. Figure 4.14 shows fabrication procedure. Argon plasma treatment was carried out under the condition that process pressure was 0.7 Pa and gas flowing rate was 50 sccm for 70 seconds. Argon plasma was exited by source power of 1500 W. Then, B_2H_6 was flown under the same condition in section 4.3.1.1. Sheet resistance by four-point probe and the thickness of amorphous-Si layer by SE were performed to investigate this purpose.

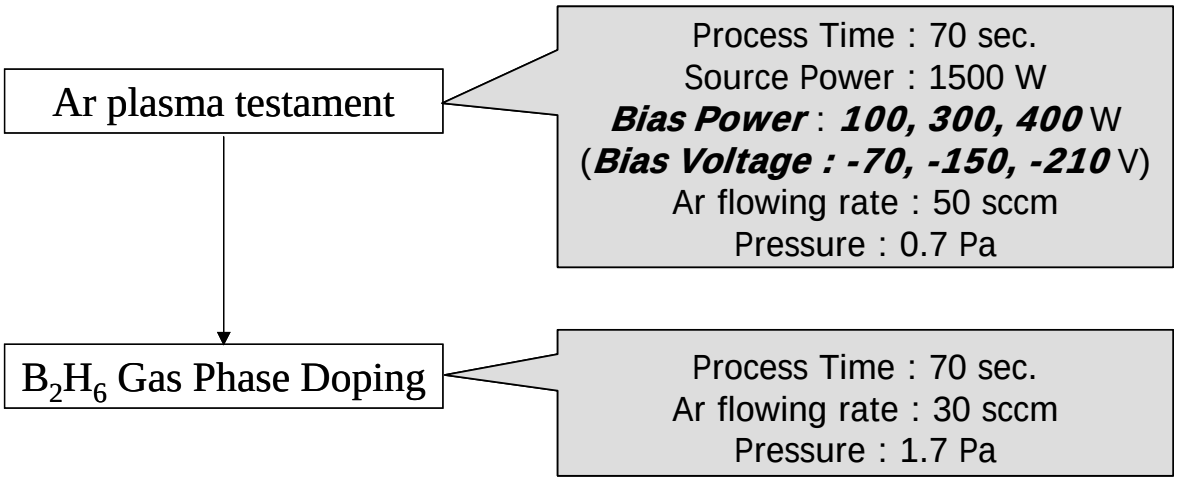

Fig.4.14 Fabrication procedure

Evaluation

boron depth profile and Sheet resistance of fabrication sample was measured by SIMS and four-point probe, respectively. Figure 4.15 shows boron depth profile by varying bias voltage by SIMS measurement. Amount of boron dose was 1.2×10^{14} and 2.8×10^{14} (atoms/cm^2) for bias voltage of –70 and -150 V, respectively. Depth of penetrated boron was about 4.6, 5.2 nm at dosage of 10^{18} (atoms/cm^2), respectively. Dosage and depth of penetrated boron were increased with increase bias voltage.

Figure 4.16 shows relation with sheet resistance and bias voltage. The result was

obtained that sheet resistance was decreased with increase bias voltage. It is suggested that dosage of boron was increased with increase bias voltage because the condition of B_2H_6 gas flowing of was same for all samples.

Table 4.1 shows the thickness of amorphous-Si by SE measurement. It was estimated that the thickness of amorphous-Si for bias voltage of –70 V, -150 V and -210V was 2.8 nm, 4.8 nm and 4.6 nm, respectively. It should be noted that amorphous-Si layer was not increased with increase bias voltage, and was deferent from depth of boron by SIMS. It is suggested that the ratio of completely amorphous-Si layer (100 % a-Si): defective amorphous-Si layer (void layer) with void was different depending on bias voltage. It is reported that top and bottom layer are grown defective amorphous-Si and completely amorphous-Si layer by Argon plasma, and thickness of void is a little changed and that of 100 % a-Si is increased even if bias voltage is increased [15-16]. Therefore, it is suggested that inverted thickness or thickness from SIMS profile can be obtained because the index of reflection of 100 % a-Si is larger than that of Si, and analysis of the layer thickness by SE is calculated from nd (n: index of reflection, d; layer thickness). Thickness by SE measurement needs to interpret ballpark estimate.

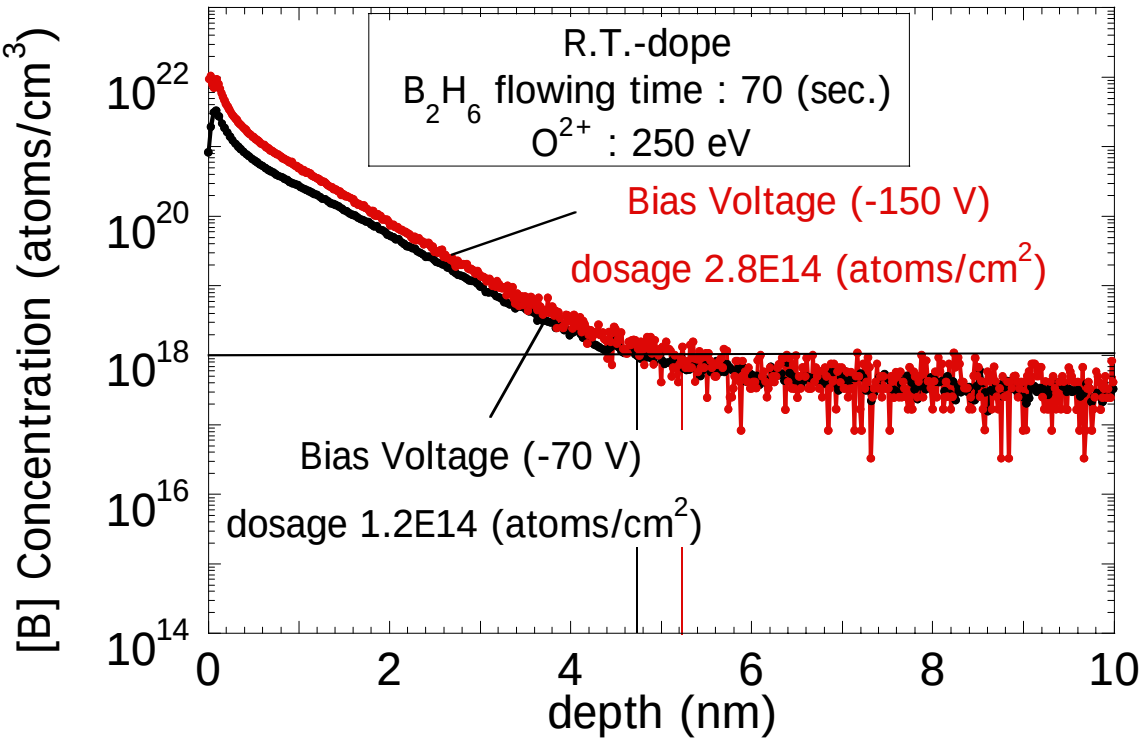

Fig.4.15 Boron depth profile by varying bias voltage by SIMS measurement

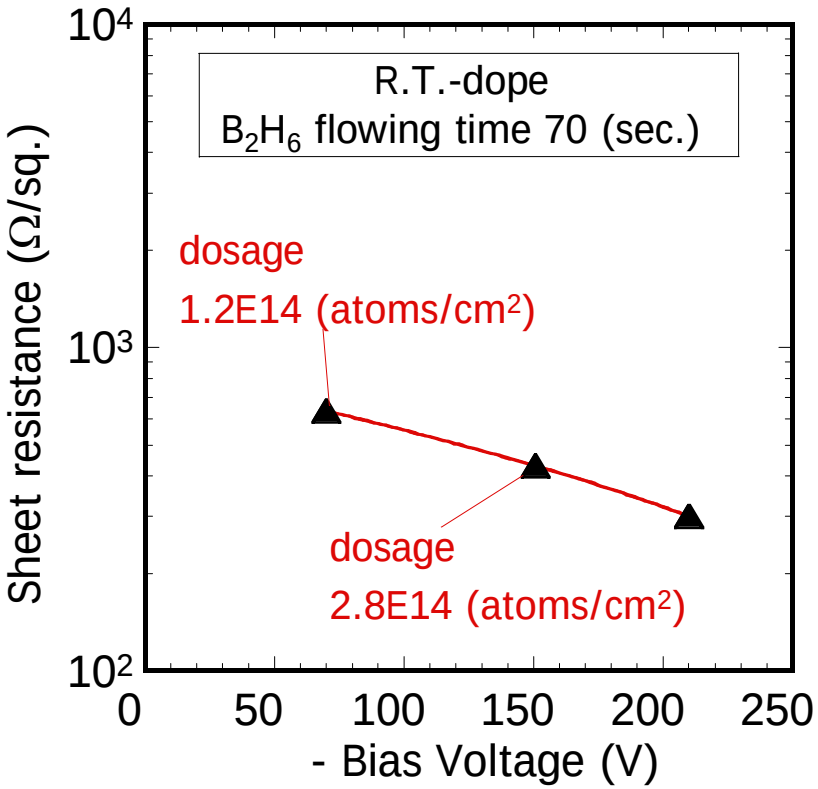

Fig.4.16 Relation between sheet resistance and bias voltage

Table 4.1 a-Si thickness by SE

Analysis model	Bias Voltage (V)	SiO_2 (nm)	a-Si (nm)
SiO_2/a-Si (kk-analysis)	-70	0.2	2.0
	-150	0.2	4.8
	-210	0.1	4.6

4.4 Summary of this chapter

Boron absorption

It was found that boron absorption was occurred without Ar plasma treatment before Gas Phase Doping at Room Temperature. It was observed that concentration of negligible surface and dosage of boron was increased with increase Ar plasma treatment, respectively. It was speculated Si-Si bonds were gradually exposed and boron was absorbed with increase of Ar plasma treatment time.

Sheet resistance was increased with Ar plasma treatment time of 5 to 10 seconds, and was gradually decreased with that of 10 to 70 seconds. It is suggested that electrical conducting layer was not formed because doping concentration was low for Ar plasma treatment time of 5seconds, and then p type layer was gradually formed by boron absorption and penetration. Figure 4.17 shows relation with sheet resistance and Ar plasma treatment time at bias voltage of –70 V and –150 V, respectively. It was found that sheet resistance gradually was decreased after Ar plasma treatment time of 10 seconds.

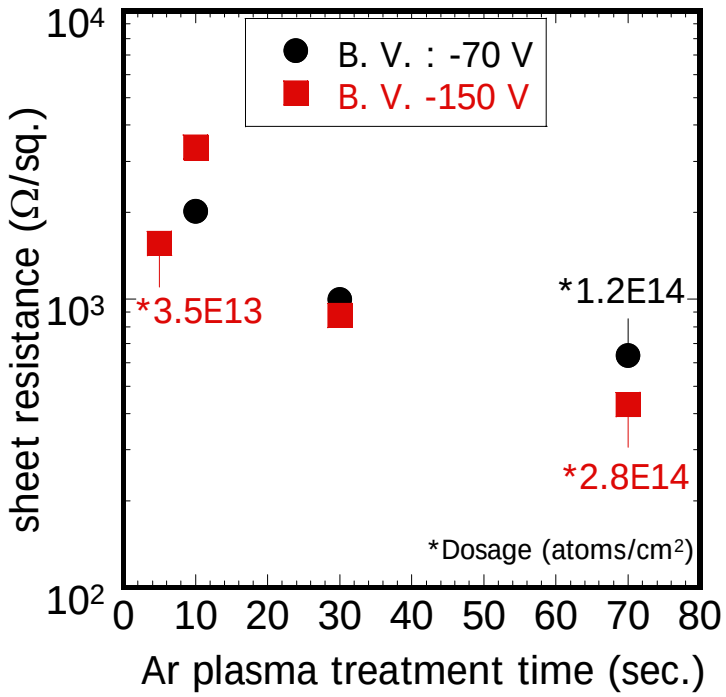

Fig.4.17 relation with sheet resistance and Ar plasma treatment time at bias voltage of –70 V and –150 V, respectively

Boron penetration

Not only sheet resistance was decreased but also depth of boron penetration was increased with increase bias voltage of Ar plasma. Thickness of a-Si and damaging layer by cross-section TEM were approximately the same as thickness of boron penetration observed by SIMS.

Figure 4.18 shows mechanisms about boron absorption or penetration. It is indicated that borons are absorbed any longer due to H-terminated of surface when Ar plasma treatment isn't carried out, boron absorption and penetration is beginning in case of short process time or small bias voltage of Ar plasma, and boron absorption and penetration is caused in case of long process time or large voltage of Ar plasma. It was found that amount of dose was dominated by absorption phenomenon, and a-Si and damaging layer in Si surface dominated depth of penetrated layer.

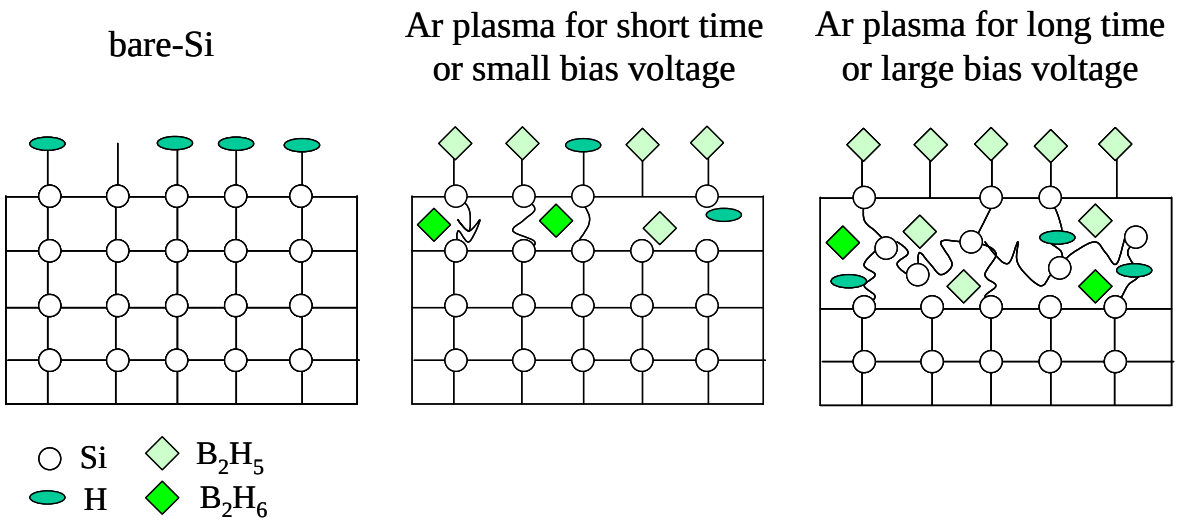

Fig.4.18 schematic of mechanism about boron absorption or penetration.

Chapter 5

Conclusions

5.1 Introduction

In this chapter, the results obtained from this work are summarized, and conclusions are described.

5.2 Summary of this study

5.2.1 Stability of High-k Gate Thin Films in Moisture Ambience

The moisture absorption tests for high-k thin films were carried out. Not only rare earth metal oxides but also ZrO_2 was degraded in moisture ambience. Various hydrocarbons were dissolved from the acryl apparatus from TDS measurement. It was found by XPS measurement that there is a possibility that entire rare earth oxide was carbonated. It was confirmed that the degradation was completely suppressed by gate electrode coverage. The hygroscopic problem of the high-k films could be solved by the gate electrode coverage. However, long-term reliability test in electrical characteristics is necessary.

5.2.2 Ultra-Shallow Junction Technology by Plasma Doping Method

In this study, it was acquired the knowledge about mechanism of reacting absorption of gas phase. It was found that borons were absorbed on the substrate surfaces, and that borons were penetrated to a-Si layers and damaging layers, by SIMS and cross-section TEM observation.

Absorption phenomenon was caused by exposed Si-Si bonds due to Ar plasma treatment for 5 seconds or more on substrate surfaces. Though this phenomenon occurred without Ar plasma treatment, as the sheet resistance by four-point probe, it was found that conducting layer was not formed.

5.3 Future Issues

It is necessary to control of dosage by not only plasma doping method and but also gas phase doping method due to relying on this study.

And so, it is necessary to estimate ultra-shallow junction formation combined with laser annealing.

References

[1] R. H. Dennard et al., “Design of ion-implanted MOSFETs with very small physical dimensions”, IEEE J. Solid-State Circuits, vol. SC-9, no. 2 pp. 256-258, 1974.

[2] Semiconductor Industry Association et al., “International Technology Roadmap for Semiconductors”, 2002 edition.

[3] Yudong Kim et al., “Conventional n-channel MOSFET devices using single layer HfO_2 and ZrO_2 as high-k gate dielectrics with polysilicon gate electrode”, IEDM Tech. Dig., 2001, pp.455-458.

[4] M. Koyama et al., “Thermally Stable Ultra-Thin Nitrogen Incorporated ZrO_2 Gate Dielectric Prepared by Low Temperature Oxidation of ZrN”, IEDM Tech. Dig., 2001, pp.459-462.

[5] E.P. Gusev el al., “Ultra high-k gate stacks for advanced CMOS devices”, IEDM Tech. Dig., 2001, pp.451-454.

[6] C. Hobbs et al., “80 nm Poly-Si Gate CMOS with HfO_2 Gate Dielectric”, IEDM Tech. Dig., 2001, pp.651-654.

[7] Sanghun Jeon et al, “Excellent Electric Characteristics of Lanthanide (Pr, Nd, Sm, Gd, and Dy) Oxide and Lanthanide-doped Oxide for MOS Gate Dielectric Applications”, IEDM Tech. Dig., 2001, pp.471-474.

[8] H. J. Osten et al., “Epitaxial Praseodymium Oxide: A New High-K Dielectric”, Ext. Abst. IWGI, 2001, pp.100-106.

[9] S. Ohmi et al., “High Quality Ultrathin La_2O_3 Films for High-k Gate Insulator”, Proc. ESSDERC’01, pp.235-238.

[10] Gin-ya Adachi, “Science of Rare Earths”, Kagaku-Dojin Co., Ltd., pp. 270-297

[11] S. Kim, “Detailing Modeling of Source/Drain Parastics and Their Impact on MOSFETs Scaling”, International Workshop on Junction Technology (IWJT) 2002, PP. 1-4,

[12] Y. Sasaki, “Helicon Wave Plasma Doping System”, IWJT 2002, pp. 37-38

[13] Y. Sasaki, “Gas Phase Doping at Room Temperature”, IWJT 2002, pp. 39-40

[14] B. Mizuno, “プラズマドーピング技術”, 応用物理, 第 70 巻, 第 12 号, 2001

[15] 石井昌彦, “ダイレクトリコイル表面計測法による半導体表面状態の評価”, 豊田中央研究所 R&D レビュー, Vol. 31 No. 1, 1996

[16] Y. Z. Hu, “In situ investigation of silicon surface cleaning and damage by argon electron cyclotron resonance plasmas”, App. Phys. Lett. 64 (10), 7 March, 1994

Acknowledgements

The author would like to give the greatest thanks to Professor Hiroshi Iwai got his thorough instruction.

The author would like to thank Associate Professor Kazuo Tsutsui for his extensive advice, valuable discussions and continuous supports.

The author would like to thank Associate Professor Hiroshi Ishiwara for his extensive advice, valuable discussions and continuous supports.

The author would like to thank Associate Professor Shun-ichiro Ohmi for his extensive advice, valuable discussions and continuous supports.

The author would like to thank Mr. Bunji Mizuno for his extensive advice, valuable discussions and continuous supports.

The author would like to thank Mr. Yuichiro Sasaki for his extensive advice, valuable discussions and continuous supports.

The author would like to thank Dr. Koji Aizawa very much who supported his researches.

The author would like to thank Mr. Takenori Kurita very much who supported his researches.

The author would like to thank Dr. Tetsuji Yano very much who supported his researches.

The author would like to thank Mr. Dai. Shouji very much who supported his researches.

The author would like to thank Mr. Satoshi Genseki for support TEM observation.

The author would like to thank Mr. Hisataka Canada very much who supported his researches.

The author would like to thank Mr. Ichiro Nakayama very much who supported his researches.

The author would like to thank Mr. Katsumi Okashita very much who supported his researches.

The author would like to thank Dr. Toshio Kudo very much who supported his researches.

The author would like to thank Dr. Cheng-Guo Jin very much who supported his researches.

The author would like to thank Mr. Akio Kometani very much who supported his researches.

The author would like to thank Mr. Sumikazu Yoshikawa for support SIMS measurement..

The author would like to thank Mr. Takashi Kouzaki for support TEM observation.

The author would like to thank Dr. Seiji Inumiya for support SE measurements.

The author would like to thank Mr. Ryouta Higaki for his kind instruction and active discussion for the experiment.

The author would be much grateful to all members of Professor Ishiwara, Tokumitu, Tsutsui, Sakai and Ohmi Laboratory, for their providing with the use of their equipments and taking care of them.

The author would like to thank research colleagues of Professor Iwai's Laboratory, Mr. J. Tonotani, Mr. K. Ohshima, Mr. Y. Kim, Mr. Jin Aun NG, Mr. K. Sato, Mr. M. Takeda, Ms. C. Ohshima, Ms. I. Kashiwagi, Mr. A. Kikuchi, Mr. J. Taguchi, Mr. H. Yamamoto, Mr. I. Ueda, Mr. A. Kuriyama, Mr. Y. Yoshihara and Mr. Hendriansyah Sauddin for the kind friendship and active discussions.

The author would like to express science gratitude to laboratory secretaries, Ms. N. Sato, Ms. Y. Mihara, Ms. K. Kubo, Ms. M. Nishizawa, Ms. K. Takahashi, Ms. E. Huruya, Ms. K. Matsuno, Ms. N. Iizuka and Ms. N. Hayashi.

This study was partially supported by STARC (Semiconductor Technology Academic Research Center). The author would like to thank Drs. N. Nakayama, T. Nishikawa, T. Arikado, J. Yugami, T. Kitano, T. Kato and K. Fujita for useful discussions and advice for this study.

This study was partially supported by Grant-in-Aid for Science Research Priority Areas (A): Highly Fictionalized Global Interface Integration.

Finally, the author would like to thank his parents, brother and brother for their warm supported and encouragement.

Sadahiro Akama,
Yokohama,
March 2003.

Appendix A

Relation between bias power and bias voltage

Bias voltage was measured by varying bias power in Argon plasma condition of Argon flow rate of 50sccm, pressure of 0.7 Pa and source power of 1500 W as shown in Fig.A1 (a). As a result, bias voltage was linearly increased with increase bias power from 100 W to 400W. While, bias voltage was implied sign of saturation when bias power was raised 400W to 500W. Therefore, in this study, bias power from 0 W to 400 W was used. Additionally, plot of Solid Square shows relation between bias power and bias voltage with auto matcher.

On the other hand, Bias voltage was measured by varying bias power in plasma mixing of B_2H_6 and Helium (He) under plasma condition of B_2H_6/He flow rate of 2/198 sccm, pressure of 0.9 Pa and source power of 1500 W as shown in Fig.A.1 (b), too. However, bias voltage was decreased with increase of bias power from 400 W to 500 W, this phenomenon was observed in case of equipment of auto matcher.

Alternatively, it was obtained that bias voltage in case of equipment with auto matcher was higher than that of without auto matcher because loss of bias voltage was suppressed drastically by reflected wave.

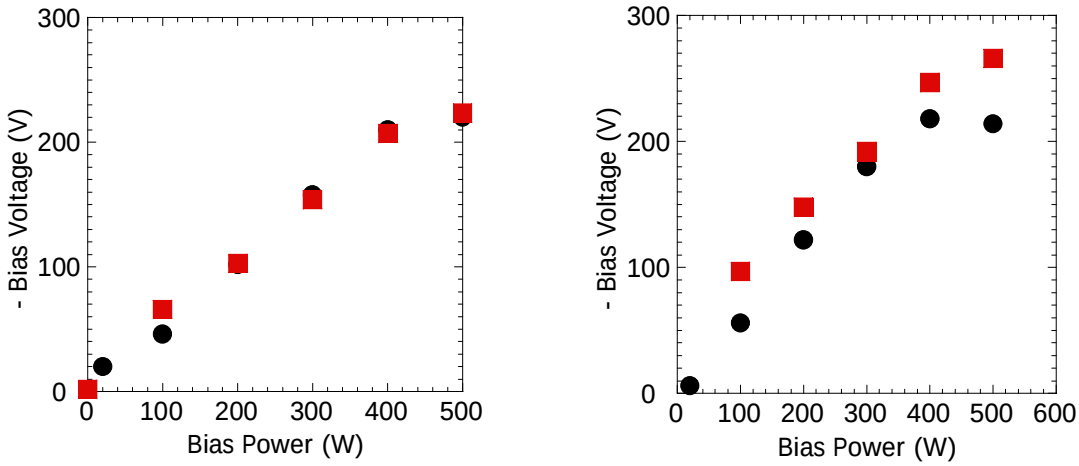

Fig.A.1 Relation between bias power and bias voltage by (a) Ar plasma and (b) mixing plasma of B_2H_6 and He

Appendix B

Plasma characteristics

Electron temperature of 2.8 eV was obtained from Langmuir probe I-V measurements for Argon plasma. It shows that this condition is weakly ionized plasma state mixed neutral atomic and molecule because electron temperature of fully ionized plasma is 15.8 eV.

Therewithal, ion density as shown in Fig.B.1 was measured at Ar flowing rate of 50-sccm and process pressure of 0.7 Pa. FigB.1 (a) shows ion density of dependence on in/out current of electromagnets at source power of 1500 W. When in/out current electromagnets was 0 A/0 A, 20 A/20 A, 40 A/40 A and 60 A/60 A, respectively, ion density was 1.65×10^{11} cm^{-3}, 1.80×10^{11} cm^{-3}, 1.75×10^{11} cm^{-3} and 1.65×10^{11} cm^{-3} at center of wafer, respectively. Uniformity of ion density was 8.44 %, 5.66 %, 5.39 % and 5.39 % within 200 nm wafers, respectively. Ion density was decreased with increase of current of electromagnets was large except for 0 A/0 A. Additionally, in that of 0 A/ 0 A, uniformity was not good. On one hand, Ion density of dependence on source power was shown in Fig.B.1 (b) at current of electromagnets of 20 A/20 A. When source power was 500 W, 1500 W, 2500 W and 3000 W, respectively, ion density was 4.06×10^{10} cm^{-3}, 1.80×10^{11} cm^{-3}, 3.15×10^{11} cm^{-3} and 3.61×10^{11} cm^{-3} at center of wafer, respectively. Uniformity of ion density was 8.34 %, 5.66 %, 4.48 % and 3.33 % within 200 nm wafers, respectively. Ion density was increased and uniformity was improved with increase source power.

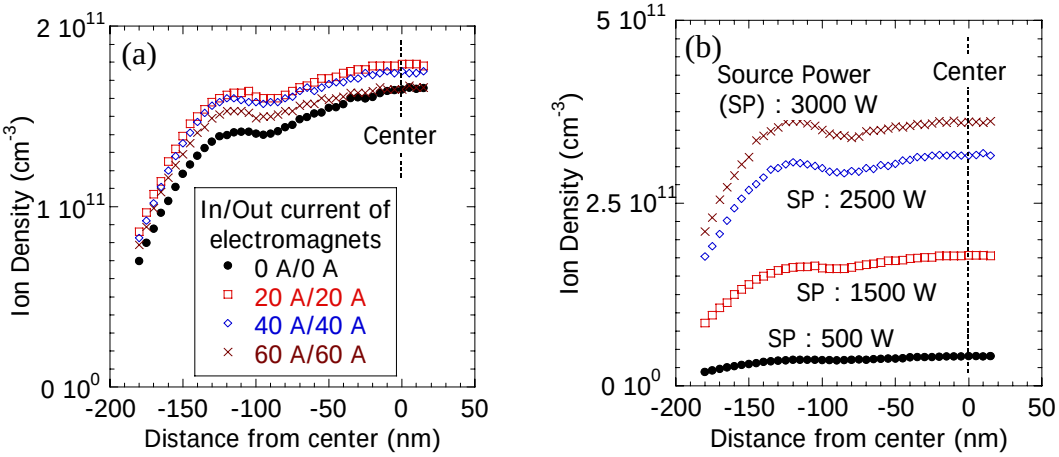

Fig.B.1 Ion density profiles of dependence on (a) current of electromagnets and (b) source power in Ar plasma.

Appendix C

Knock-on effect by the primary ion energy of SIMS measurement

Experimental thickness of Boron penetration by SIMS tends to estimate thicker than real thickness due to thrust of impurity called knock-on effect by a primary ion (in this study, O^{2+}). Knock-on effect is increased with increase primary ion energy. It is necessary to be small primary ion energy in order to obtain accurate boron depth profile.

Figure C.1 shows relation between a primary ion energy and Boron depth profile by SIMS measurement. It was obtained the result that depth of boron penetration was decreased with decrease primary ion energy. When O^{2+} ion energy was 300eV and 500eV, depth of boron penetration was 4.6 nm and 6.6 nm, respectively. Therefore, it is suggested that real depth of Boron penetration was less than 4.6 nm in view of knock-on effect.

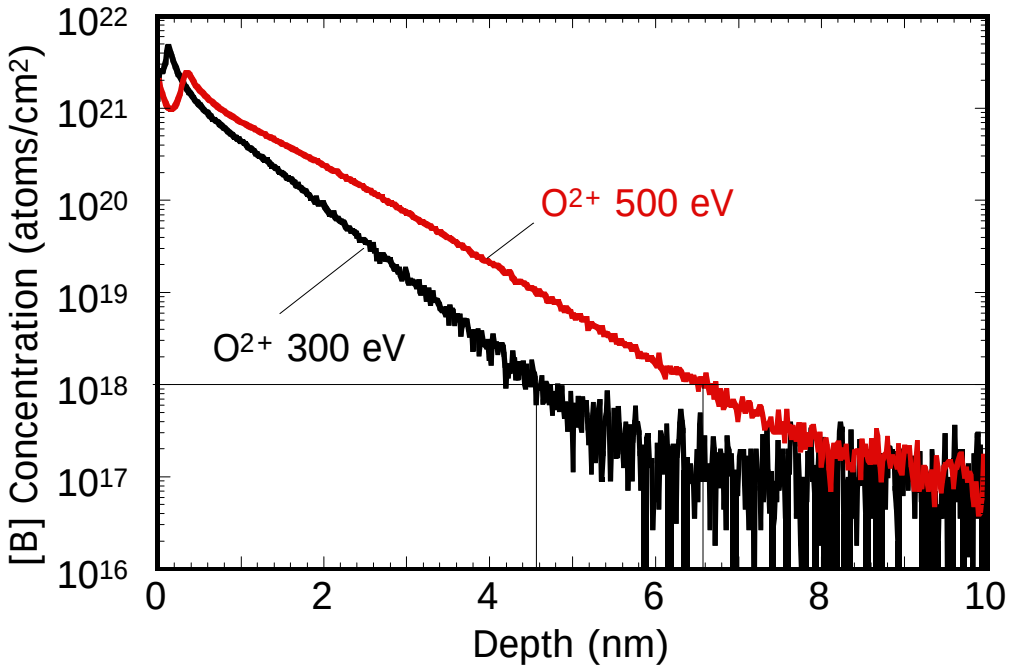

Fig.C.1 A primary ion energy (O^{2+}) dependence on Boron depth profile